Nonpeptide Inhibitors of Measles Virus Entry

Aiming Sun,[†] Andrew Prussia,[†] Weiqiang Zhan,[†] Ernest E. Murray,[†] Joshua Doyle,[‡] Li-Ting Cheng,[‡] Jeong-Joong Yoon,[‡] Eugene V. Radchenko,[§] Vladimir A. Palyulin,[§] Richard W. Compans,[‡] Dennis C. Liotta,[†] Richard K. Plemper,[‡] and James P. Snyder*[,†]

Department of Chemistry, Emory University, 1515 Dickey Drive, Atlanta, Georgia 30322, Department of Microbiology & Immunology, Emory University School of Medicine, 3086 Rollins Research Center, 1510 Clifton Road, Atlanta, Georgia 30322, and Department of Chemistry, Moscow State University, Moscow 119992, Russia

Received March 6, 2006

Measles virus (MV) is one of the most infectious pathogens known. Despite the existence of a vaccine, over 500 000 deaths/year result from MV or associated complications. Anti-measles compounds could conceivably reverse these statistics. Previously, we described a homology model of the MV fusion protein trimer and a putative binding site near the head−neck region. The resulting model permitted the identification of two nonpeptidic entry inhibitors. Here, we present the design, synthesis, and bioevaluation of several series of fusion inhibitors and describe their structure-activity relationships (SAR). Five simply substituted anilides show low-μM blockade of the MV, one of which (AS-48) exhibits $IC_{50} = 0.6-3.0$ μM across a panel of wild-type MV strains found in the field. Molecular field topology analysis (MFTA), a 2D QSAR approach based on local molecular properties (atomic charges, hydrogen-bonding capacity and local lipophilicity), applied to the anilide series suggests structural modifications to improve potency.

Introduction

Paramyxoviruses are negative stranded RNA viruses, most of which are highly contagious airborne pathogens that spread via the respiratory route. Members of this viral family include major human and animal pathogens such as measles virus (MV[a]), human parainfluenza viruses (HPIV), mumps virus, respiratory syncytial virus, and Newcastle disease virus.[1] Despite the existence of an effective live-attenuated vaccine,[2] MV remains a serious threat to human health globally, accounting for approximately 0.5 million deaths annually.[3] Although most of these cases occur in developing countries with limited access to vaccination, measles outbreaks still occur in some developed countries that have failed to maintain high vaccine coverage rates.[4,5] The very recent rash of infections and deaths in Romania is a case in point.[6] Other recent outbreaks, in particular in the U.K., have been attributed to declining herd immunity as a result of reduced vaccination coverage resulting from parental concerns about vaccination safety.[7] Furthermore, vaccine-induced immunity is less robust than naturally acquired protection, which may result in a progressive loss of immunity in adults in fully vaccinated populations that are not subject to natural boosting through circulating virus.[8−10] Taken together, these facts make desirable the development of novel therapeutics that can be used for the rapid control of local outbreaks and improved case management to limit severe outcomes of infection.

MV infects through pH-independent fusion of the viral envelope with the plasma membrane of target cells.[11,12] The process is initiated by an interaction of the hemagglutinin (H) envelope glycoprotein with its cellular receptor, either the regulator of complement activation CD46 or the signaling lymphocyte activation molecule (SLAM/CD150w). Although the MV vaccine strains of the Edmonston lineage efficiently use CD46 as their cellular receptor,[13,14] most wild-type strains of MV are dependent on SLAM for efficient entry.[15−17] Receptor binding is thought to trigger H to activate the fusion (F) envelope glycoprotein, which through a series of conformational changes mediates membrane merger, resulting in the release of the viral genome into the target cell.[1,11]

Interfering with virus entry is an attractive therapeutic strategy for controlling virus infection and spreading. Proof-of-principle for the clinical benefit of this approach has been demonstrated most notably by the efficacious peptidic HIV inhibitor enfuvirtide (T-20).[18,19] Other peptides possess considerable in vitro potency against retroviruses and paramyxoviruses, including HPIV types 2 and 3,[20,21] MV,[20] respiratory syncytial virus,[20] Sendai virus,[22] and Newcastle disease virus.[23] Although confirming the therapeutic benefit of entry inhibitors for the treatment of viral infections, T-20 has highlighted potential obstacles that complicate large-scale production of peptide-based antivirals. Large peptides such as T-20 are, in many cases, difficult to solubilize and purify, making manufacture highly cost intensive. Such peptides generally show poor absorption and bioavailability from the GI tract, necessitating delivery through injection. Furthermore, virus-derived peptides have the potential to be immunogenic in vivo and may induce adverse events in some cases.

In view of these obstacles, we aimed to explore the inhibitory potential of nonpeptidic small molecules against MV entry. Conceptual support for this approach emerged during the course of our work as other groups identified small molecules that interfere with respiratory syncytial virus (RSV) entry in vitro[24] and in vivo.[24−26] In previous work, we reported the structure-based development of a MV entry inhibitor, *N*-(5-amino-2-hydroxyphenyl)-2-phenylacetamide (AM-4, **7a**, Table 2), with an IC_{50} of 260 nM against the MV vaccine strain MV-

* Corresponding author. Phone: 404-727-2415. Fax: 404-727-6586. E-mail: jsnyder@emory.edu.

[†] Department of Chemistry, Emory University.

[‡] Department of Microbiology & Immunology, Emory University School of Medicine.

[§] Moscow State University.

[a] Abbreviations: MV, measles virus; RSV, respiratory syncytial virus; NDV, Newcastle disease virus; HPIV, human parainfluenza virus; F-trimer, fusion protein trimer; SLAM, signaling lymphocyte activation molecule; CPE, cytopathic effect; MV-Edm, measles virus Edmonston strain; HR-B, heptad repeat domain B; AS48, lead molecule **11f**; CC_{50}, cytotoxicity concentration at 50% maximal dose; SAR, structure-activity relationship; QSAR, quantitative structure-activity relationship; MFTA, molecular field topology analysis.

10.1021/jm0602559 CCC: $33.50
Published on Web 08/03/2006

Table 1. Antiviral MV IC_{50} values for Monosubstituted Acetanilides **1a**, **3**, and **4**[a]

entry	compd	Y, R_2[b]	IC_{50} (μM)[c]	IC_{50}-res[d]	CC_{50}[e]	SI[f]
1	**1a**		55	>**150**	>**600**	>**10**
2	**3a**	C, *m*-NO_2	8.5	ND	>600	>71
3	**3b**	C, *p*-NO_2	16	ND	550	34
4	**3c**	C, *o*-NO_2	>100	ND	>600	ND
5	**3d**	C, *o*-COOH	60	ND	>600	>10
6	**3e**	C, *m*-OH	25	ND	>600	>24
7	**3f**	C, *o*-OH	13	>150	525	40
8	**3g**	C, *m*-CN	6.5	>150	>600	>92
9	**3h**	N, 5-F	109	ND	>600	>6
10	**4a**	C, *m*-NH_2	19	>150	>600	>32
11	**4b**	C, *p*-NH_2	135	ND	>600	>4

[a] See Scheme 1. [b] The *o*-, *m*-, and *p*- designations refer to substitution relative to NHCO. [c] The IC_{50} concentrations were calculated for suppression of virus-induced cytopathicity (CPE) against the MV Edmonston strain as detailed in the Experimental Section. [d] The IC_{50} concentrations of selected compounds against a MV variant resistant to inhibition by AS-48 because of a point mutation at position 462 in the F protein.[30] ND: not determined. [e] CC_{50}: cytotoxicity concentration at 50% maximal dose. [f] Selectivity index (CC_{50}/IC_{50}).

Table 2. Antiviral MV IC_{50} values for Disubstituted Phenol Series **7**[a]

entry	compd	R_4,[b] M, R_5	IC_{50} (μM)[c]	CC_{50}[d]	SI[e]
1	**7a**[f]	*m*-NH_2, CH_2, H	0.26	17	65
2	**7b**	*p*-NH_2 , CH_2, H	75	>600	>8
3	**7c**	*p*-NH_2, CH_2O, H	[g]	ND	ND
4	**7d**	*m*-NO_2, CH_2, H	47	450	10
5	**7e**	*m*-NO_2, CH_2, *m*-OMe	>100	>600	ND
6	**7f**	*m*-NO_2, CH_2, *p*-OMe	>100	600	<6
7	**7g**	*m*-NO_2, CH_2O, H	>100	600	<6
8	**7h**	*p*-NO_2, CH_2O, H	>100	>600	ND
9	**7i**	*m*-$CONH_2$, CH_2, H	127	>600	>5
10	**7j**	*m*-COOMe, CH_2, H	66	>600	>9
11	**7k**	*m*-CF_3, CH_2, H	>100	>600	ND

[a] See Scheme 2. [b] The *m*- and *p*- designations refer to the substitution relative to NHCO. [c] The IC_{50} concentrations were calculated for the suppression of virus-induced cytopathicity (CPE) against the MV Edmonston strain as detailed in the Experimental Section. [d] CC_{50}: cytotoxicity concentration at 50% maximal dose. [e] Selectivity index (CC_{50}/IC_{50}). [f] Ref 27. [g] Not active below the cytotoxic dose.

Edmonston (MV-Edm).[27,28] Because this compound proved to be unstable, we developed AS-48 (**11f**, Table 3) as a shelf-stable alternative. A screening of a panel of viral isolates representing MV strains of all genotypes currently endemic worldwide revealed effective inhibition of most isolates by this substance.[29] To further elucidate the basis of inhibition and better understand the mechanism of MV glycoprotein-mediated fusion, we generated and characterized resistant MV variants.[30] Spontaneous mutations conferring drug resistance were confirmed in transient assays and in the context of recombinant virions and were in all cases located in the fusion protein. Several mutations emerged independently at F position 462, which is located in the *C*-terminal heptad repeat (HR-B) domain. The data support the conclusion that residues located both in the head domain of the F trimer and the helical HR-B region contribute jointly to controlling F conformational stability.

In the current study, we describe the preparation of a series of AS-48 analogues and develop SARs based on both the MV F-protein homology model and molecular field topology analysis (MFTA).[31,32]

Preliminary F-Protein Pocket SAR. Our homology model of the MV fusion protein based on the crystal structure of the Newcastle disease virus fusion protein[33] reveals a cylinder-like cavity near the interface of the head and neck region formed by residues that play a critical role in the cytopathicity of MV.[27,28] With approximate dimensions of 10 Å in diameter and

Table 3. Antiviral MV IC_{50} values for Disubstituted Nitro Series **11** and Anilines **14**[a]

entry	compd	R_3	IC_{50}, μM[b]	IC_{50}-res[c]	CC_{50}[d]	SI[e]
1	**11a**	*p*-OH	63	ND	>600	>10
2	**11b**	*p*-F	>100	ND	450	<5
3	**11c**	*m*-NO2	30	>150	>600	>20
4	**11d**	*o*-benzyl ester	68	75	75	1
5	**11e**	*m*-NH_2	11	>150	>600	>55
6	**11f**[f]	*o*-$CONH_2$	3	>150	325	108
7	**11g**	*m*-$CONH_2$	3.7	>75[g]	170	46
8	**11h**	*m*-NHOH	6	>75[g]	325	54
9	**11i**	*m*-COOMe	4	>150	440	110
10	**11j**	*m*-COOH	5	>150	>600	>120
11	**11k**	*m*-CH_2OH	6	>150	>600	>100
12	**14a**	*m*-$CONH_2$	18	ND	>600	>33
13	**14b**	*m*-COOH	55	ND	>600	>11
14	**14c**	*m*-NH_2	>100	ND	ND	ND

[a] cf. Scheme 5. [b] The IC_{50} concentrations were calculated for the suppression of virus-induced cytopathicity (CPE) against the MV Edmonston strain as detailed in the Experimental Section. [c] The IC_{50} concentrations of selected compounds against an MV variant resistant to inhibition by AS-48 because of a point mutation at position 462 in the F protein.[30] ND: not determined [d] CC_{50}: cytotoxicity concentration at 50% maximal dose. [e] Selectivity index (CC_{50}/IC_{50}). [f] AS-48. [g] The 75 μM highest concentration assessed because of the cytotoxicity of the compounds.

depth, a hydrophobic floor and a hydrophilic rim (Figure 1), the cavity guided us in the identification of the lead benzoxazole **1a** (OX-1[27]). The compound shows low cytotoxicity, specifically inhibits live MV-Edm and MV glycoprotein-induced membrane fusion with an $IC_{50} = 55$ μM, and interferes with F-mediated membrane fusion and, hence, viral entry as the molecular basis for inhibition.[27] The overall features of the three-center docking model are depicted for **1a** in Figure 1. The optimally docked ligand locates the unsubstituted phenyl ring deep in the hydrophobic pocket and presents two polar groups near the cavity rim for hydrogen-bonding interactions. The NH_2 moiety is presumed to interact with Glu339, whereas the oxazole oxygen is within 1.8−2.0 Å of the cationic terminus of Arg268.

The applicability of the docking model was initially verified with a small set of benzoxazoles (**1**) and aromatic amides (**3**).[27] For example, relative to that of **1a**, compounds **1b** and **1c** show reduced activity compatible with structural alterations that impair docking at the target site (Figure 1). Structure **1c** lacks the conformational flexibility necessary for the terminal phenyl ring to achieve beneficial hydrophobic contact with the base of the pocket, whereas **1b** orients its benzoxazole ring in the same position, but misses the NH_2— Glu339 hydrogen bond (model not shown). Additional support for the binding model came from the finding that second-generation molecules designed for better shape and charge complementarity to the pocket possess greatly increased antiviral activity. For example, **4a**, an acyclic analogue of **1a**, replaces the oxazole ring oxygen with the superior proton-accepting amide carbonyl group improving the blockade of MV fusion by 5-fold (Table 1).

In the following, we describe a number of compound series that take inspiration from the cavity docking model depicted in Figure 1. Despite the compatibility of the structures and the docking motif, it should be noted that although our current data support the model, we do not yet have direct proof (e.g., photoaffinity labeling) that our compounds bind to the cavity depicted. Furthermore, it is possible that the blockade of MV fusion could arise from the existence of more than one binding site for compound docking. We do, however, provide evidence that the compounds described below inhibit MV replication by interfering with MV-fusion events. As detailed in Tables 1 and 3, 12 compounds with IC_{50} values ranging from 3 to 70 μM

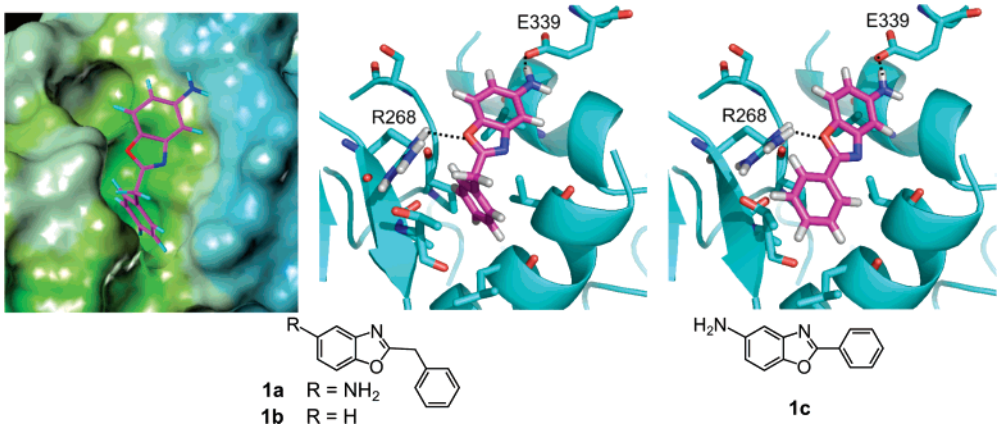

Figure 1. Molecular dynamics refined docking models of benzoxazole **1a** and **1c** in an MV fusion protein binding pocket. The left surface representation and middle secondary structure views both apply to **1a.**

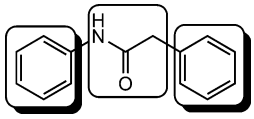

Figure 2. Three sectors of 2-phenylacetanilide subjected to synthetic modification as an approach to measles virus entry blockers.

have been tested against an MV variant resistant to inhibition by AS-48[30] (**11f**, Table 3). As measured by IC_{50}-res, extensive cross-resistance was observed in all cases, providing strong support for the notion that active members of the anilide series interfere with viral entry. In addition, we have ruled out cytotoxicity as the origin of MV replication blockade by determining 50% cytotoxic concentrations (CC_{50}, Tables 1−3). The corresponding selectivity indices (CC_{50}/IC_{50}) for 9 of the 10 compounds range from >20 to >120.

Acetanilide Synthesis. Although small library screening based on a geometric analysis of the MV fusion protein Val94-centered binding pocket yielded benzoxazole **1a** as the original hit, chemistry resources were quickly focused on acyclic variants as depicted in Schemes 1−4. Recognizing that the oxazole oxygen is a rather poor hydrogen-bond acceptor, the amide carbonyl was preferred as the far better proton acceptor for interaction with Arg268 in the three-point binding model. Accordingly, the SAR evolved by examination of the three molecular fragments circumscribed in Figure 2, namely, the anilide ring on the left, the amide linker, and the distal phenyl ring on the right.

Sector 1: Acetanilide Phenyl Ring. The monosubstituted acyclic acetanilides **3** and **4** were readily prepared by treatment of substituted anilines **2** with phenyl acetyl chloride in THF using pyridine as the base. In most cases, reaction yields were essentially quantitative. Reduction of the NO_2 group in **3a** and **3b** by hydrogenation over 5% Pd/C afforded anilines **4a** and **4b**, respectively (Scheme 1, Table 1).

Preparation of a second series of disubstituted benzamides was guided by the characteristics of the model-binding pocket and the SAR that emerged from the monosubstituted analogues (see below). In particular, an OH group was located ortho to the amide by combining substituted 2-hydroxy anilines **5** with various phenyl acetyl chlorides **6** to give **7d**−**k** as depicted in Schemes 2, 3 and Table 2. Hydrogenation of the nitro analogues

Scheme 1

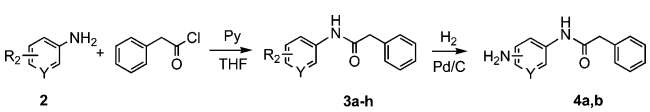

Scheme 2

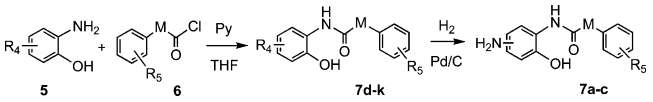

Scheme 3

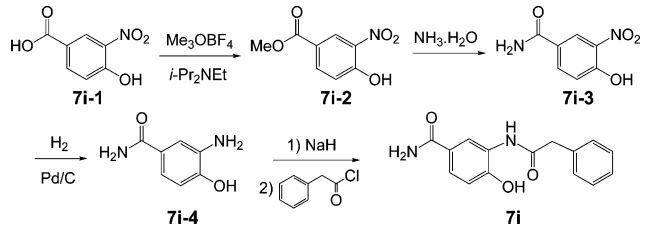

Scheme 4

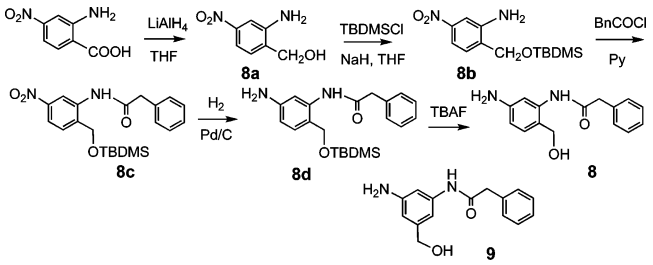

over Pd/C delivered anilines **7a**−**c**. Given the instability of **7a**, presumably due to oxidation of the masked hydroquinone, a methylene group was installed between the OH and the aromatic ring to give **8** as shown in Scheme 4. Analogue **9** was prepared by a similar route.

Preparation of a third set of disubstituted congeners, each incorporating a nitro group meta to the aromatic amide center (**11a**−**k**), began with **10** and employed the same straightforward method as that used for series **7**. Isomers **11f** and **11g** incorporate an amide group ortho and meta, respectively, relative to the amide center. The corresponding benzoic acids **12a**,**b** were separately treated with thionyl chloride to provide the acetyl chlorides, followed by treatment with ammonium hydroxide at 50 °C for 25−30 h to deliver **13a**,**b**. The latter were then combined with phenyl acetyl chloride to afford compounds **11f**,**g**. Hydrogenation of **11g** over Pd/C delivered product **14a** (Scheme 5).

Sector 2. Distal Phenyl Ring. Preliminary attempts to introduce substituents into the benzyl ring were made by modifying the structure of **3a** to obtain halogen analogues **15**−**17** and pyridines **18**−**20** by standard coupling procedures

Scheme 5

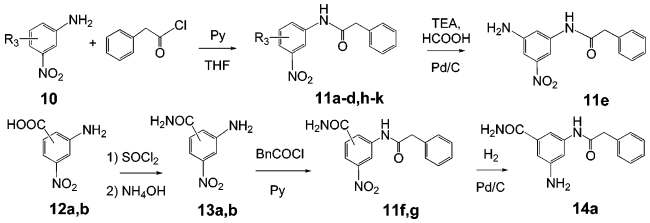

employing acid chlorides.

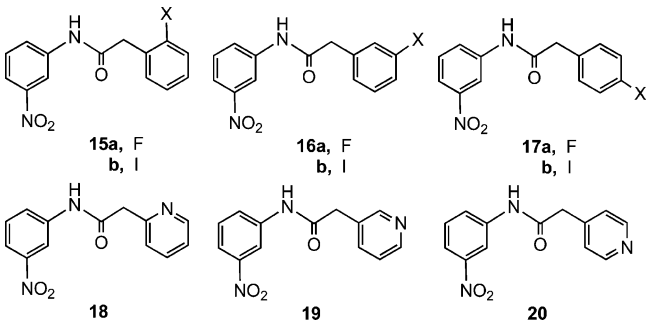

Intermediate Linker Region. Three variations were cursorily examined as exemplified by **7g**, **21**, and **22** (Experimental Section). Each was prepared without complication by procedures outlined in the Experimental Section.

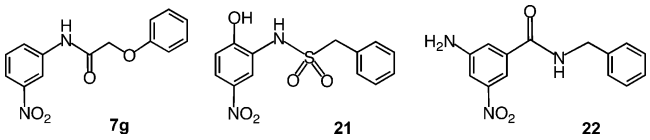

F-Protein Homology Model SAR. Sector 1: Acetanilide Phenyl Ring. The binding model of benzoxazole inhibitor lead **1a** (Figure 1) depicts the aniline NH_2 as a rather strong hydrogen-bond donor to Glu339 and the oxazole oxygen as a weak H-bond acceptor from Arg268. As a consequence, we anticipated that the monosubstituted anilines **4a** and **4b** (Table 1) combined with the amide carbonyl would improve activity. To our delight, the intermediate *m*-nitro compound **3a** exhibits an approximate 2-fold improvement in IC_{50} in the anti-MV assay in comparison with that of the *m*-NH_2 analogue **4a**.

Simplistically, it would appear that the anilino phenyl ring adopts conformations that maximize the binding in each case. Thus, the *m*-NH_2 in **4a** is directed at Glu339 as in **1a**, whereas the *m*-NO_2 in **3a** interacts with Arg48 and Ser45. Figure 3

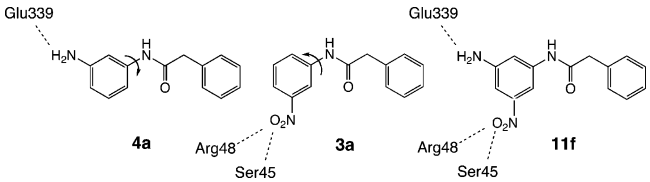

Figure 3. Idealized orientation of proton-donating and proton-accepting meta substituents in the substituted acetanilides.

captures the situation. It might be expected that combining the two nitrogen substituents in the same molecule would reinforce the action of both. Unfortunately, this is not the case because **11f** (Scheme 5, Table 3) proves to be similar in activity to **4a** (Table 1), suggesting that the nitro group as pictured for **3a** in Figure 3 is the dominant interaction. Not surprisingly, the doubly substituted dinitro and diamino analogues (**11c** and **14c**, respectively; Table 3) are inactive in comparison.

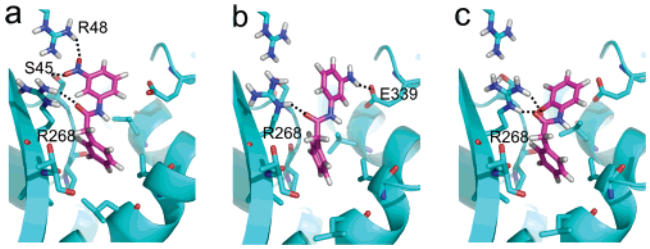

Figure 4. Docking models for **3a**, **4a**, and **3f**. (a) The amide C═O and *m*-NO_2 of **3a** accept an H-bond from Ser45, whereas *m*-NO_2 is likewise H-bonded to Arg48. (b) The *m*-NH_2 of **4a** acts as a proton donor to Glu339. (c) The amide C═O and *o*-OH of **3f** accept H-bonds from Arg268.

The explicit docking model for **3a** suggests that the amide C═O interacts with Arg268, whereas the *m*-NO_2 groups interact simultaneously with Ser45 and Arg48 (Figure 4a). Compound **3b** bearing a *p*-NO_2 is about 10-fold less active, consistent with the meta-to-para shifted nitro group residing in a less favorable receptor subsite relative to the arginine residues, whereas the very poor *o*-NO_2 analogue **3c** is undoubtedly compromised by an unfavorable conformation. The meta-to-para shift observation is likewise obtained for the amino group (i.e., **4a** to **4b**, Table 1), resulting in a 27-fold reduction in activity accompanied by the displacement of NH_2 away from Glu339. The nitro functionality is generally less prized as a hydrogen bond-acceptor in comparison with other lone-pair-bearing groups. However, X-ray crystal structure determinations for nitro-bearing small molecules embedded in protein binding sites make it clear that the nitro substituent is capable of playing this role.[34]

It is instructive to compare the docked complexes of *m*-NO_2 **3a** and *m*-NH_2 **4a**. As portrayed in Figure 4b, compound **4a**'s interaction with residues of the pocket involves a different rotamer of the substituted aromatic ring in contrast to that suggested by Figure 3. However, although the comparison implies a 180° rotation, the actual angles predicted for the optimized complexes are ϕ(C(O)N-CC)'s of −38° (**3a**) and −145° (**4a**), a relative change of 107°. The implication is that the doubly substituted analogue **11e** cannot simultaneously fulfill the needs of both moieties at any given torsional angle, thus explaining the lack of additivity for the individual substituents. The fact that **11e** is not quite as active as *m*-NO_2 **3a** presumably arises because of the greater desolvation penalty for **11e** (4.1 kcal/mol relative to that of **3a** by AMSOL SM5.4 calculation[35]) so that *m*-NH_2 does not achieve a fully compensatory interaction with Glu339.

Exchange of *m*-NO_2 with *m*-CN (i.e., **3a** to **3g**) retains activity around 6 μM, presumably due to cyanide H-bonding with Arg48. A meta-OH does not sustain the same level of activity (**3e**, 25 μM, Table 1), the hydroxy oxygen falling between the two active site arginines, but the ortho-analogue recovers 2-fold (**3f**, 13 μM) by virtue of a productive interaction with Arg268. In the corresponding model of the complex (Figure 4c), the phenyl ring adopts yet a third rotational angle (ϕ(C(O)N-CC) = −46°). The replacement of the anilide phenyl ring with a fluoro-substituted pyridine ring (**3h**) causes the activity to drop precipitously.

The hydroxy-bearing disubstituted anilide series **7** (Scheme 2) took its inspiration from the isolation of **7a** during the preparation of **1a**. The compound exhibits an IC_{50} of 260 nM (Table 2) and an ideal docking model (Figure 5a), but its instability in air both in the NMR tube and under assay conditions[29] rules it out as a therapeutic candidate. Our first attempt to bypass the presumed hydroquinone-like oxidation of the anilide ring involved the replacement of the *o*-OH in **7a**

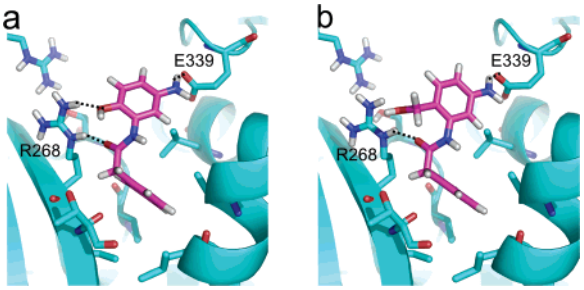

Figure 5. Docking models for **7a** and **8**. (a) Compound **7a** places its phenyl ring in the hydrophobic pocket and satisfies two-center H-bonding with 3 groups. (b) Compound **8** loses its CH_2OH H bond to R268.

with *o*-F (structure not shown). However, the compound had no measurable antiviral activity at concentrations up to 300 μM.

Consequently, we turned to a number of other analogues that retained the *o*-OH but placed various substituents at other ring positions as shown in Scheme 2. At 47 μM, compound **7d** was the most active analogue (Table 2). An additional attempt to take advantage of an OH group in this region of the molecule is depicted in Scheme 4. A multistep synthesis was employed to replace the *o*-OH with *o*-CH_2-OH to give **8**, thereby eliminating the hydroquinone moiety in the anilide ring. A similar route was employed for the meta-analogue **9**. Although both compounds proved to be shelf-stable, unfortunately they had no antiviral activity at concentrations up to 100 μM.

Docking of **8** in the F-protein pocket (Figure 5**b**) suggests that the origin of inactivity is a ligand conformation that prevents the CH_2OH and the C═O groups from simultaneously interacting with Arg268, while shifting the structure somewhat out of the pocket. As a result, Arg48 and Ser 45 are too distant to interact with the CH_2OH group. The activity of **8** also suffers from a high internal strain energy (8.6 kcal/mol relative to the global minimum), a value rather high in comparison to the quantity for **7a** (1.7 kcal/mol relative to the global minimum). Further manipulation in this series was abandoned.

While evaluating phenol series **7** (Scheme 1, Table 2), we likewise pursued the nitro and aniline series **11** and **14**. Our motivation stemmed from the observation that the *m*-NO_2 analogue **3a** exhibits what appears to be productive hydrogen bonding with Arg48 and Ser45, while dominating the *m*-NH_2—Glu339 interaction of **4a**.

This series proved to be only moderately fertile, though it did lead to analogues in the low micromolar range. The most active member, **11f** (AS-48) with an *o*-$CONH_2$ unit, delivered an IC_{50} of 3 μM against the MV assay protocol employing the MV-Edmonston strain. Interestingly, the shelf-stable AS-48 has demonstrated 0.6 μM activity against several wild-type strains of the measles virus.[29] It is noteworthy that all MV wild types carry a methionine at F residue 94, whereas the Edmonston line harbors a valine at this position. It has likewise proved to be a uniquely useful reagent in the investigation of the mechanism of F-protein action during early phases of the virion-cell fusion process.[30] Compound **11g** bearing a *m*-$CONH_2$ group as well as meta-analogues **11h**—**k** are only 1.5—2-fold less active than **11f** (4—6 μM, Table 3). Surprisingly, members of this set of compounds are only slightly more active than the monosubstituted *m*-NO_2 analogue **3a** (8.5 μM, Table 1). Modeling suggested that these compounds are not able to engage the *m*-NO_2 with Arg48 and Ser45 while maintaining $CONH_2$ interaction with Glu339, a situation similar to that described above for **11f**.

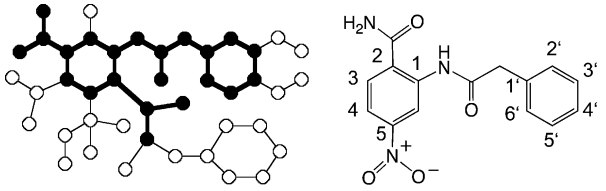

Figure 6. MFTA supergraph representing the dataset of 29 congeneric MV entry inhibitors (left) with the sample superposition of compound **11f** (AS-48) (right) on it shown with black circles and black bonds.

Sector 2: Distal Phenyl Ring. Several benzyl group modifications within the active *o*-NO_2 series were explored. Two methoxy substitutions on the benzyl group of **3a** leading to drastic loss of activity (**7e** and **7f**, Table 2) suggest the ring to be rather intolerant of substitution. The preparation of the *o*-, *m*-, and *p*-fluoro and -iodo analogues **15**—**17** confirms the observation. All iodo substitutions lead to IC_{50} values >75 μM (>300 μM for the ortho and meta cases). The fluoro analogues are somewhat more forgiving. The *o*-fluoro (**15a**) and *o*,*o*′-difluoro substances are inactive at >75 μM, whereas the meta and para derivatives **16a** and **17a** show IC_{50} values of 47 and 9 μM, respectively. Clearly, only the para-position permits substitution by a rather small hydrogen-atom replacement. An attempt to introduce polarity into the distal phenyl without adding steric bulk involved the preparation of pyridines **18**—**20**. Unfortunately, at IC_{50} values of >75μM, the ring nitrogens are clearly detrimental to blocking the fusion process. We surmise that this results because the ring nitrogens increase the desolvation penalty by 3.9—4.4 kcal/mol, without engaging in a productive polar interaction.

Intermediate Linker Region. An extension of the short linker between amide and phenyl from CH_2 to CH_2O and beyond proved deleterious in every case as illustrated by **7c**, **7g**, and **7h** (Table 2). Replacement of the anilide amide of **7d** (IC_{50} 47 μM) with NH-SO_2 to give **21** also lost activity (IC_{50} > 300 μM), as did other analogous sulfonamides. Finally, the reverse amide of **11e** (IC_{50} 11 μM), namely, **22**, showed a 2-fold loss of activity (IC_{50} 23 μM). Although none of these variations has been examined in depth, the preliminaries are not encouraging.

Molecular Field Topology Analysis (MFTA) QSAR. MFTA is an analytical method for generating quantitative structure-activity relationships (QSARs) by topological analysis of a series of compounds associated with a numerical biological endpoint.[31,32] The approach seeks to model bioactivity in terms of local molecular properties (descriptors). MFTA produces a molecular supergraph for the set of compounds examined, PLS-based correlation statistics, and a graphical representation of impact of each local descriptor on activity.

In the present application, the log(1/IC_{50}) values for 29 MV entry inhibitors (compounds **3a**—**3g**, **4a**, **4b**, **7b**, **7d**—**7f**, **7i**—**7k**, **11a**—**11k**, **14a**—**14c**; Tables 1—3) were tested against a variety of local descriptor sets (value 2*X* was used for compounds whose activity is determined as >*X*). A series of different models was constructed with predictive q^2 values (leave-25%-out cross-validation) in the range 0.32—0.53 (compound **7a** was not included in the training set because it is an outlier in all models, possibly reflecting its unusually high degree of reactivity). The molecular supergraph is shown in Figure 6 with compound **11f** superimposed on it.

The best results were obtained with the following descriptors:[32] *Q* (effective atomic charge; Gasteiger—Marsili), H-bond donor (H_d) and acceptor (H_a) ability (Abraham), and L_g (local lipophilicity; sum of Ghose—Crippen atomic contributions for an atom and attached hydrogens). The resulting correlation

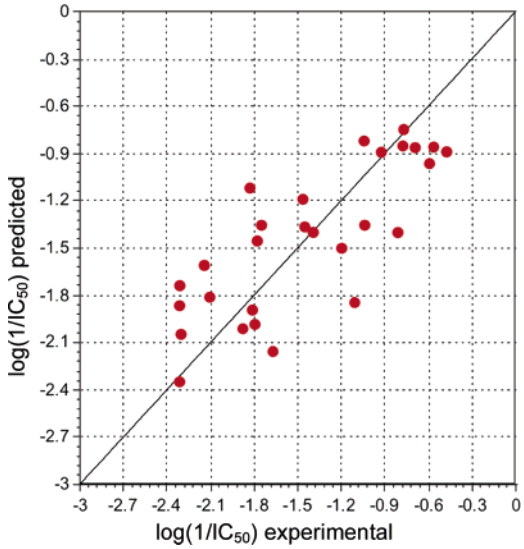

Figure 7. MFTA correlation of 29 MV entry blockers based on the following descriptors: charge (Q), H-bonding (H_a and H_d), and lipophilicity (L_g).

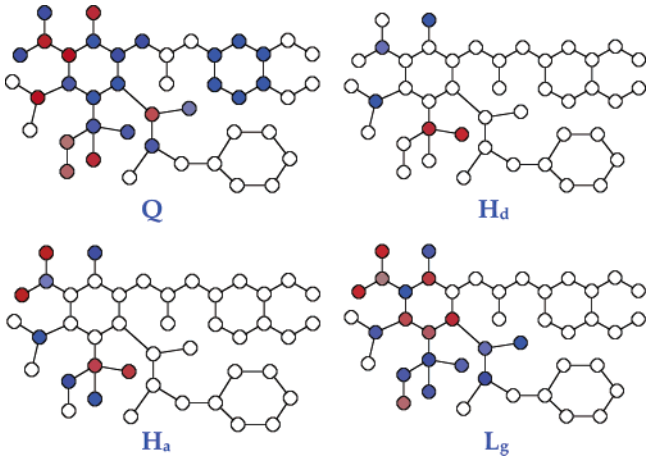

Figure 8. Impact on the activity of four local descriptors (Q, H_a , H_b, and L_g) expressed on the MV entry blocker supergraph. An increase in the descriptor property at the red and blue positions predicts an increase and a decrease in activity, respectively.

(Figure 7) is characterized by $N = 29$, number of PLS factors $N_F = 1$, $r = 0.809$, $r^2 = 0.654$, RMSE = 0.352 and $q^2 = 0.529$ (leave 25%-out cross-validation). Increasing the number of descriptors did not improve the correlation. The deletion of three outliers present in a subset of the models would certainly improve the correlation, but we decided to retain them. Despite this, the predictive ability of the correlation is acceptable.

The major contributions of the local descriptors to the correlation can be expressed in terms of color-coded supergraphs (Figure 8). At the red-colored positions, an increase in descriptor property implies an increase in activity. At the blue-colored positions, an increase suggests a decrease in activity.

The activity increase of the anilides as depicted by the supergraphs is suggested to arise from a decrease in negative charge (more positive) at the ortho- and para-anilide positions. At the same time, these centers should serve as neither H-bond donors nor acceptors. In addition, activity gains are posited if the ortho-positions are made less lipophilic. However, the analysis suggests that activity could be improved if the meta-substituents carry either an H-bond donor or an H-bond acceptor. This is consistent with meta substituents forming hydrogen bonds to Glu339 and Arg48 in the MV homology model. Furthermore, MFTA recommends that the substitution of terminal phenyl ring should avoid changes that increase partial atomic charge on the ring atoms. Indeed, increased polarity is incompatible with the ring's positioning in the hydrophobic pocket of the protein model. The latter statement comes with the caveat that an examination of additional structural variations in the phenyl terminal region is desirable in order to draw more definitive conclusions.

One additional point concerns the leave-25%-out cross-validation treatment. We regard this strategy as an excellent check of model quality because it involves using four different test sets, each of which incorporates 25% of the compounds. In the present case, the statistics result from taking the average error of predictions for the four test sets. Nonetheless, some readers may feel more comfortable with the more common construction of a full training set validated by an external test set. This experiment has been performed using a test set of nine compounds. The results (described in the Supporting Information) are entirely compatible with the model described above.

Summary and Conclusions

Our previously reported homology model of the MV fusion protein contains a cylindrical pocket in the head−neck region occupied by Val94. Certain F-protein mutants arising from the single site substitution of this residue were shown to be resistant to benzoxazole **1a** and anilide **11f**, providing evidence for the location of ligand binding. Molecular modeling as pictured in Figure 1 suggested a three-point pharmacophore characterized by a hydrophobic site, a hydrogen-bond accepting site (Arg268), and a hydrogen-bond donating site (Glu339). Using this model as a guide, we have prepared the first examples of nonpeptidic measles virus entry blockers (Schemes 1−4) and measured their ability to ablate virion-cell fusion with the Edmonston measles strain (Tables 1−3). The masked hydroquinone **7a** shows an IC_{50} value of 260 nM and presents ideally in the binding model (Figure 5a). However, the compound's instability in air, presumably resulting from oxidation to the corresponding quinone, eliminates it as an antiviral lead.

In the context of the MV-Edm assay, the remaining compounds furnish IC_{50} values ranging from low to high μM. All are compatible with the Val94 binding pocket associated with the homology model. The best analogue to date, shelf-stable **11f** (AS48, IC_{50} 3 μM, Table 3), carries nitro and amido groups meta and ortho to the anilide nitrogen, respectively. The nitro group is able to interact with Arg48/Ser45, effecting a fourth point in the pharmacophore in contrast to the other three-point systems mentioned in the previous sections (cf. Figure 3). Against other MV strains, the same compound is effective from 0.6 to 3 μM.[29]

An interesting observation arises when comparing the substitution of either NO_2 or NH_2 meta to the C-1 anilide center. Although the IC_{50} values of the monosubstituted compounds are similar (8.5 (**3a**) and 19 (**4a**) μM, respectively, Table 1), the four-point model suggests a torsional reorientation of the substituted phenyl ring to accommodate the structures (cf. Figure 3). Surprisingly, the installation of both groups on the same ring (**11e**) does not substantially affect activity (11 μM, Table 3). Similar observations can be made for the doubly substituted compounds **11f**−**k**. The removal of the R_3 group (Scheme 5) elicits only a mild reduction in the IC_{50} value (3−6 μM, Tables 1 and 3). The lack of synchrony between the meta positions of the anilide aromatic ring can be traced to the spatial disposition of the three polar contacts in the pharmacophore: the closely coupled Arg48/Ser45 residues, the Arg268 residue, and the

Glu339 residues that constitute three of the four F-protein binding pocket pharmacophore centers. The protein model suggests that the flat anilide ring is unable to simultaneously sample the three polar subsites via hydrogen bonding, adopting instead an anilide torsion angle that maximizes the interaction with the substituent that offers the strongest noncovalent interaction, that is, *m*-NO_2. The importance of the phenyl torsion is illustrated further by the reduced activity of analogues **8** and **9**, which adopt unique phenyl orientations preventing the *m*- and *o*-CH_2OH groups from participating in hydrogen-bonding (Figure 5b).

A second apparently critical feature of the SAR concerns what appears to be a rather tight hydrophobic pocket housing the phenyl ring of the distal benzyl group. Of the eight halogen and methoxy substituents (**7e**,**f** and **15**−**17**), only the *p*-F substitution **17a** delivers an IC_{50} value below 50 μM (i.e., 9 μM). Polarity in this region likewise appears to ablate fusion activity as evidenced by the inactivity of pyridines **18**−**20**. The constraints of the rather shallow pocket appear to be associated with the length and character of the linker region. Both shortening (**1b**) and lengthening the topological distance between the amide and the distal phenyl ring diminishes activity. The replacement of the amide with sulfonamide or reverse amide accomplish the same.

We have employed molecular field topology analysis (MFTA) to create a QSAR model for the MV entry blockers based on three local descriptors: atomic charge, hydrogen-bonding capacity, and group lipophilicity. Although the correlation is only of moderate quality ($r = 0.81$, $r^2 = 0.65$), the predictive capacity of the model is acceptable ($q^2 = 0.53$). Nevertheless, a preliminary interpretation of the descriptor impact on activity as expressed by the supergraphs (Figure 8) suggests structural modifications in the anilide ring that might lead to improved inhibition, while advising that certain substitutions would be detrimental. Work is underway to exploit the SAR derived from Tables 1−3 to enhance the MFTA correlation and to transform it into a predictive tool that can be used with confidence.

Finally, two recent, important, and independent observations serve to place the model in context. First, novel spontaneous resistant MV variants have been generated in response to the exposure of MV to AS-48. In all cases, these were located in the fusion protein, including the F head region within the binding cavity pictured in Figures 1 and 4 (e.g., V94) and in the distal *C*-terminal heptad repeat (HR-B) domain (e.g., N462). An analysis of the data supports the conclusion that residues located in the head domain of the F trimer and the HR-B region jointly contribute to controlling F refolding.[30] Although it may be tempting to speculate that AS-48 may alternatively or additionally bind to the heptad repeat domain, the formation of the final F fusion core structure[36,37] is not inhibited by the compound.[30]

Second, the X-ray structure of the paramyxovirus SV5 fusion protein has been solved in the metastable pre-fusion conformation[38] and shown to differ significantly from the previously resolved intermediate or post-fusion structures of hPIV3 F[39] or NDV F[33] as a consequence of a number of complex and deep-seated rearrangements. Important for the present work, a comparison of homology models of the pre- and post-fusion MV F proteins demonstrates that the binding cavity shown in Figures 1 and 4 is not present in the pre-fusion conformation of the MV F-trimer.[40] Importantly, we found that AS-48 binding enhances co-immunoprecipitation of MV F with HR-B derived synthetic peptides,[30] which is only possible when the paramyxovirus F trimer is present in a fusion-intermediate conformation.[41] Thus, the present inhibitors are most certainly blocking a transient intermediate conformation, in which the binding pocket must be sufficiently formed so that both fusion blockade and acquired mutation can be mediated by the compounds described herein. Present studies seek high potency elimination of MV fusion by tailoring the present inhibitors to the intermediate form and by simultaneously targeting the pre-fusion F trimer with a different set of compounds.

Experimental Section

Cell Culture and Production of MV Stocks. Vero (African green monkey kidney) cells were maintained at 37 °C and 5% CO_2 in Dulbecco's modified Eagle's medium (DMEM) supplemented with 10% fetal bovine serum (FBS), penicillin, and streptomycin. Vero-CD150w cells stably expressing human CD150w were incubated in the additional presence of G-418 at a concentration of 1.0 mg/mL. MV Edmonston was grown and analyzed on Vero cells, whereas for experimentation with wild-type MV isolates, Vero-CD150w cells were used. To prepare virus stocks, cells were infected at a multiplicity of infection (MOI) of 0.01 plaque-forming units (pfu)/cell and incubated at 37 °C. The cells were scraped in OPTIMEM (Invitrogen), and the virus was released by two freeze−thaw cycles. Cleared virus preparations titered by 50% tissue culture infective dose ($TCID_{50}$) determination according to the Spearman−Karber method as previously described.[29]

Dose−Response Inhibition Curves for Virus Replication. Two different assays were developed to assess the sensitivity of MV to candidate compounds. Solvent (DMSO) concentrations in both assays did not exceed 0.1%, at which no adverse effect on cell viability or virus replication could be detected. Control infections of cells in the presence of equal amounts of DMSO were nevertheless included in each experiment. In the first of two assays, compound activity was quantified on the basis of a suppression of virus-induced cytopathicity. Cells were infected in two to four replicates per compound concentration in a 96-well plate format at an MOI of 0.2 pfu/cell in the presence of compound in 2-fold dilutions with starting concentrations ranging from 75 to 300 μM (ending concentrations: 0.3−1.2 μM). At 96 h post-infection, virus-induced cytopathicity was quantified using a nonradioactive proliferation assay (Promega) and results calculated according to the formula for the cytopathic effect (% rel. CPE = 100-(experimental-background)/(maximum-background)*100). Results presented in Tables 1−3 are based on the above-described cytopathicity assay. Selected compounds were reexamined in a second cell-based viral replication assay[27] to determine effective concentration based on virus yields for confirmation. Cells were infected at a multiplicity of infection (MOI) of 0.2 plaque forming units (pfu)/cell in the presence of compound in 2-fold dilutions with starting concentrations ranging from 75 to 300 μM and incubated in the presence of compound at 37 °C for 36 h. Cell-associated viral particles were then harvested as described above and virus titers determined by $TCID_{50}$ titration. For all compounds analyzed in both assays, the results were compatible (data not shown). Furthermore, all experiments were performed in multiple replicates. For IC_{50} calculations, dose−response curves were generated on the basis of average values derived from these replicates. Plotting of individual curves (exemplified for compound **11f** (AS-48); see Supporting Information, Figure S2) did not reveal significant changes in IC_{50} values, reflecting the low degree of variation.

In a final set of experiments, IC_{50} values for selected compounds were examined in the virus-induced cytopathicity assay using a MV variant resistant to inhibition by **11f** (AS-48) because of a point mutation at position 462 in the F protein.[30] In all cases analyzed (cf. Tables 1 and 3), extensive cross-resistance was observed, strongly arguing that all active members of this compound series interfere with viral entry.

Cytotoxicity Determination. To determine compound-associated cytotoxicity, cells were incubated in the presence of compound in 2-fold dilutions with starting concentrations of 600 μM (ending concentration: 2.3 μM) for 36 to 40 h. Cellular proliferation still in the presence of compound was then determined over 1 h using

the same nonradioactive proliferation assay (Promega) as described above. Cytotoxicity was determined in two independent replicates. The corresponding curves were generated on the basis of average values derived from these replicates. Plotting of individual curves for each replicate (exemplified for compound **11f** (AS-48); see Supporting Information, Figure S3) did not reveal significant changes in CC_{50} values, reflecting the low degree of variation between individual replicates. Selectivity indices (CC_{50}/IC_{50}) are provided in Tables 1−3.

Chemistry. Mass spectrometric analysis was provided by the Emory University Mass Spectrometry Center. Routine proton and carbon NMR spectra measured during synthesis were obtained on Varian Inova-400 (400 MHz) or Varian Inova-600 (600 MHz) spectrometers. The solvents for NMR were deuteriochloroform ($CDCl_3$) (residual shifts: δ 7.26 for ^{1}H and δ 77.2 for ^{13}C) and deuteriodimethyl sulfoxide (DMSO-d_6; residual shift: δ 2.5 for ^{1}H and δ 39.51 for ^{13}C). The residual shifts were taken as internal references and reported in parts per million (ppm). TLC and preparative thin-layer chromatographies (PTLC) were performed on precoated, glass-backed plates (silica gel 60 F_{254}; 0.25 mm thickness) from EM Science and were visualized by a UV lamp. Column chromatography was performed with silica gel (230−400 mesh ASTM) using the flash method. Elemental analyses were performed by Atlantic Microlab, Inc. Norcross, Georgia. All solvents and other reagents were purchased from Aldrich Chemical Co., Milwaukee. The reagents were used as received.

Compound 1a. A mixture of 2,4-diaminophenol dihydrochloride (1.36 g, 10 mmol), phenylacetic acid (1.36 g, 10 mmol) and PPA (15 g) was heated slowly to 110 °C with stirring until the heavy foaming ceased, then heated to 210 °C. The reaction was kept at this temperature for 2.5 h. The solution was cooled to 100 °C, poured into 500 mL of ice water, neutralized to pH = 8, and extracted by Et_2O several times. The product was purified by chromatography to obtain a light brown solid, yield 65%.

^{1}H NMR (600 MHz, $CDCl_3$) δ 3.61 (2H, br), 4.19(2H, s), 6.59 (1H, dd, J = 2.4 Hz, 8.4 Hz), 6.94 (1H, d, J = 2.4 Hz), 7.19 (1H, d, J = 8.4 Hz), 7.23−7.35 (5H, m). HRMS calcd for $C_{14}H_{12}N_2O$, 224.09496; found, 224.09571 M^+.

General Procedures for the Synthesis of Compound Series 3. Aniline (**2**, 1.0 mmol) was treated with pyridine (1.1 equiv, 1.1 mmol) in THF at room temperature for 10 min, followed by the addition of phenylacetyl chloride (1.0 equiv, 1.0 mmol) at 0°C. The reaction mixture was warmed to room temperature for 2 h and then filtered. The filtrate was poured into aqueous NH_4Cl (saturated aqueous) and extracted with ethyl acetate (3×). The combined organic phases were dried over Na_2SO_4. The products were purified by chromatography or recrystallization.

General Procedure for the Hydrogenation of NO_2-amides to NH_2-amides. Nitro-subsituted amides (1.0 equiv, 1 mmol) were treated with H_2 (50 psi) for 3−10 h in the presence of Pd/C (5 mmol %, 0.05 mmol). The reaction was monitored by TLC until the starting material was no longer detected. The Pd/C residue was removed by filtration, followed by rotary evaporation of the solvent. The crude product was further purified either by flash chromatography or by recrystallization.

***N*-(3-Nitrophenyl)-2-phenylacetamide (3a).** From 3-nitroaniline (1 mmol, 138 mg), phenylacetyl chloride (1 mmol, 155 mg), and pyridine (1.1 mmol, 87 mg), the general procedure gave **3a** as a yellow solid in quantitative yield. ^{1}H NMR (400 MHz, $CDCl_3$) δ 3.79 (2H, s), 7.34−7.48 (6H, m), 7.89 (1H, dd, J = 1.2 Hz, 8.4 Hz), 7.94 (1H, dd, J = 1.6 Hz, 8.2 Hz), 8.22(1H, dd, J = 2.0 Hz, 2.0 Hz). Anal. Calcd for $C_{14}H_{12}N_2O_3$: C, 65.62; H, 4.72; N 10.93. Found: C, 65.47; H, 4.71; N, 10.78.

***N*-(4-Nitrophenyl)-2-phenylacetamide (3b).** From 4-nitroaniline (1 mmol, 138 mg), phenylacetyl chloride (1 mmol, 155 mg), and pyridine (1.1 mmol, 87 mg), the general procedure delivered **3b** as a yellow solid in quantitative yield.^{1}H NMR (400 MHz, $CDCl_3$) δ 3.81 (2H, s), 7.33−7.46 (6H, m), 7.60 (2H, d, J = 9.2 Hz), 8.17 (2H, d, J = 9.2 Hz). Anal. Calcd for $C_{14}H_{12}N_2O_3$: C, 65.62; H, 4.72; N 10.93. Found: C, 65.50; H, 4.72; N, 10.82.

***N*-(2-Nitrophenyl)-2-phenylacetamide (3c).** The general procedure gave product **3c** as a yellow solid: R_f = 0.61 (2:1, hexane/ethyl acetate). ^{1}H NMR (400 MHz, $CDCl_3$) δ 10.28 (1H, s), 8.80 (1H, dd, J = 2 Hz, 0.3 Hz,), 8.16 (1H, dd, J = 2 Hz, 0.4 Hz,), 8.37 (1H, dt, J = 2 Hz, 0.4 Hz,), 7.36−7.47 (5H, m), 7.13 (1H, dt, J = 2 Hz, 0.4 Hz,), 3.84 (2H, s); ^{13}C NMR (100 MHz, $CDCl_3$) δ 170.51, 136.10, 134.92, 133.46, 129.87, 129.56, 128.21, 125.90, 123.53, 122.20, 46.03. Anal. Calcd for $C_{14}H_{12}N_2O_3$: C, 65.62; H, 4.72; N, 10.93. Found: C, 65.60; H, 4.70; N, 10.88.

2-(2-Phenylacetamido)benzonic Acid (3d). The general procedure gave product **3d** as a white solid :^{1}H NMR (400 MHz, DMSO-d_6) δ 11.15 (s, 1H), 8.50 (d, J = 2 Hz, 1H), 7.94 (dd, J = 2 Hz, J = 0.4 Hz, 1H), 8.37 (dt, J = 2 Hz, J_2= 0.4 Hz, 1H), 7.23−7.36 (m, 5H), 7.13 (dt, J = 2 Hz, J = 0.4 Hz, 1H), 3.76 (s, 2H); ^{13}C NMR (100 MHz, DMSO-d_6) δ 169.59, 169.40, 140.81, 134.84, 134.07, 131.07, 129.55, 128.60, 127.01, 122.73, 119.85, 116.37, 44.68. Anal. Calcd for $C_{15}H_{13}NO_3$: C, 70.58; H, 5.13; N, 5.49. Found: C, 70.45; H, 5.12; N, 5.54.

***N*-3-Hydroxyphenyl-2-phenylacetamide (3e) (AS-114).** From 3-amino-phenol (5 mmol, 546 mg), phenylacetyl chloride (5 mmol, 770 mg), and pyridine (5.5 mmol, 435 mg), the general procedure gave **3e** as a light yellow solid. ^{1}H NMR (400 MHz, DMSO-d_6) δ 3.59 (2H,s), 6.42 (1H, dd, J = 1.2 Hz, 8.0 Hz), 6.94 (1H, d, J = 8.0 Hz), 7.03 (1H, d, J = 8.0 Hz), 7.17−7.32 (6H, m), 9.36 (1H, s), 10.02 (1H, s). Anal. Calcd for $C_{14}H_{13}NO_2$: C, 73.99; H, 5.77; N, 6.16. Found: C, 73.32; H, 5.68; N, 6.10.

***N*-2-Hydroxyphenyl-2-phenylacetamide (3f) (AS-113).** From 2-amino-phenol (5 mmol, 546 mg), phenylacetyl chloride (5 mmol, 770 mg), and pyridine (5.5 mmol, 435 mg), the general procedure gave **3f** as a light yellow solid (488 mg, 43% yield).^{1}H NMR (400 MHz, DMSO-d_6) δ 3.78 (2H, s), 6.72−6.75 (1H, dd, J = 7.8 Hz, 7.8 Hz), 6.83 (1H, d, J = 6.8 Hz), 6.92 (1H, dd, J = 7.2 Hz, 4.0 Hz), 7.23−7.36 (5H, m), 7.76 (1H, d, J = 7.6 Hz), 9.38 (1H, s). Anal. Calcd for $C_{14}H_{13}NO_2$: C, 73.99; H, 5.77; N 6.16. Found: C, 73.96; H, 5.78; N, 5.91.

***N*-(3-Cyanophenyl)-2-phenylacetamide (3g).** A mixture of 3-amino-benzonitrile (2 mmol, 236.3 mg) and $NaHCO_3$ (2.2 mmol, 185 mg) in $CHCl_3$ (10 mL) was stirred at room temperature for 10 min, followed by the addition of phenylacetyl chloride (2.1 mmol, 323.4 mg). The reaction rapidly changed color from brown to white as a white solid precipitated. After stirring for 2 h, the reaction mixture was poured into 10 mL of H_2O and extracted with CH_2Cl_2 (3× 5 mL). The combined organic layers were dried over Na_2SO_4 and purified by chromatography to give **3g** as a white solid (354 mg, 75%). ^{1}H NMR (400 MHz, $CDCl_3$) δ 3.79 (2H, s), 7.14 (1H, br), 7.25−7.44 (7H, m), 7.60−7.62 (1H, m), 7.82(1H, s). Anal. Calcd for $C_{15}H_{12}N_2O$: C, 76.25; H, 5.12; N 11.86. Found: C, 75.84; H, 5.00; N, 11.54.

***N*-(5-Fluoropyridin-2-yl)-2-phenylacetamide (3h) (AS-128).** From 2-amino-5-fluoropyridine (0.5 mmol, 56 mg), phenylacetyl chloride (0.5 mmol, 77 mg), and pyridine (0.6 mmol, 47.4 mg), after 48 h at room temperature, the general procedure provided compound **3h** as a white solid (96 mg, 84% yield). 1H NMR (400 MHz, $CDCl_3$) δ 3.79 (2H,s), 7.26−7.38 (3H,m), 7.39−7.41 (3H,m), 7.78 (1H,s), 8.05 (1H,d, J = 2.8 Hz), 8.24 (1H,dd, J = 4.4 Hz, 11 Hz). Anal. Calcd for $C_{13}H_{11}FN_2O$: C, 67.82; H, 4.82; N, 12.17. Found: C, 67.47; H, 4.76; N, 12.02.

***N*-(3-Aminophenyl)-2-phenylacetamide (4a) (AM-5).**[27] Hydrogenation of **3a** following the general procedure for the reduction of the nitro group to an amine delivered **4a** as a light yellow solid in 85% yield. ^{1}H NMR (400 MHz, $CDCl_3$) δ 3.78 (2H, s), 6.40 (1H, dd, J = 2.67 Hz, 8.0 Hz), 6.51 (1H, dd, J = 2.70 Hz, 6.4 Hz), 6.93 (1H, br), 7.02(1H, t, J = 8.0), 7.09(1H, br), 7.32−7.42(5H, m). Anal. Calcd for $C_{14}H_{14}N_2O$: C, 74.31; H, 6.24; N 12.38. Found: C, 74.15; H, 6.24; N, 12.27.

***N*-(4-Aminophenyl)-2-phenylacetamide (4b).** Hydrogenation of **3b** following the general procedure gave **4b** as a light yellow solid in 85% yield. ^{1}H NMR (400 MHz, $CDCl_3$) δ 3.75 (2H, s), 6.60 (2H, d, J = 8.8 Hz), 6.90(1H, s), 7.16 (2H, d, J = 8.8 Hz), 7.32−7.41 (5H,m). Anal.Calcd for $C_{14}H_{14}N_2O$: C, 74.31; H, 6.24; N, 12.38. Found: C, 73.47; H, 6.35; N, 11.89.

***N*-(5-Amino-2-hydroxyphenyl)-2-phenylacetamide (7a) (AM-4).**[27] Pyridine (0.869 g) was mixed with 2-amino-4-nitrophenol (1.54 g) in anhydrous tetrahydrofuran (10 mL) on ice, followed by the addition of phenylacetyl chloride (1.69 g). The precipitate was washed with ammonium chloride (sat. aq) and extracted with ethyl acetate, and the combined extracts were dried over anhydrous sodium sulfate. The dried extract (2.72 g) was solubilized in methanol, hydrogenated (50 psi (1 psi = 6.89 kPa)), and the combined filtrates were washed with methanol. The product was purified by chromatography with hexane and ethyl acetate (1:2) as the eluant; 70% yield. ^{1}H NMR (600 MHz, $CDCl_3$) δ 3.80 (s, 2H), 6.27 (d, J = 1.8 Hz, 1H), 6.46 (dd, J = 2.4 Hz, 7.2 Hz, 1H), 6.80 (d, J = 8.4 Hz, 1H), 7. 33−7.44 (m, 5H).

***N*-(4-Amino-2-hydroxyphenyl)-2-phenylacetamide (7b) (B17-E3).** Using the procedure described for **7a**, compound **7b** was obtained as a purple solid in 80% yield. ^{1}H NMR (600 MHz, DMSO-d_6) δ 3.63 (2H,s), 4.85 (2H,s), 5.97 (1H,dd, J = 2.4 Hz, 8.4 Hz), 6.09 (1H,d, J = 2.4 Hz), 7.10 (1H, d, J = 9 Hz), 7.22−7.32 (m, 5H), 9.24 (1H,s), 9.30 (1H,s). Anal. Calcd for $C_{14}H_{14}N_2O_2$: C, 69.41; H, 5.82; N, 11.56. Found: C, 68.95; H, 5.99; N, 11.49.

***N*-(4-Amino-2-hydroxyphenyl)-2-phenoxyacetamide (7c) (AS-10).** Using the procedure described for **7a**, **7c** was obtained as yellow solid in 80% yield. ^{1}H NMR (600 MHz, $CDCl_3$) δ 4.63 (2H,s), 6.22 (1H,d, J = 8.4 Hz), 6.37 (1H,s), 6.77 (1H,d, J = 8.4 Hz), 6.99 (1H,d, J = 9 Hz), 7.08 (1H, m), 7.36 (1H,m), 8.35 (1H,s), 8.86 (1H,br). Anal. Calcd for $C_{14}H_{14}N_2O_3$: C, 65.11; H, 5.46; N, 10.85. Found: C, 64.91; H, 5.52; N, 10.65.

***N*-(2-Hydroxy-5-nitrophenyl)-2-phenylacetamide (7d) (B17-E4).** From 4-nitro-2-amino-phenol (10 mmol, 1.54 g), phenylacetyl chloride (10 mmol, 1.55 g), and pyridine (11 mmol, 0.87 g), the general procedure for series **3** gave **7d** as a yellow solid. The compound was used as an intermediate for the synthesis of **7a** without further purification. ^{1}H NMR (400 MHz, $CDCl_3$) δ 3.82 (2H,s), 7.03 (1H,d, J = 8.8 Hz), 7.35−7.49 (m,5H), 7.81 (1H,d, J = 2.8 Hz), 7.99 (1H,dd, J = 2.8 Hz, 9.2 Hz), 10.05 (1H, s); HRMS calcd for $C_{14}H_{12}N_2O_4$ 272.0797; found, 271.0724 $[M - H]^+$.

***N*-(2-Hydroxy-5-nitrophenyl)-2-(3-methoxyphenyl)acetamide (7e) (AS-40).** From 2-amino-4-nitro-phenol (2.5 mmol, 335 mg), 3-methoxyphenylacetyl chloride (2.5 mmol, 461.6 mg), and pyridine (3 mmol, 237 mg), the general procedure for **3** provided **7e** after stirring at room-temperature overnight; yellow solid (103 mg, 14% yield). ^{1}H NMR (400 MHz, $CDCl_3$) δ 3.61(2H,d, J = 4.4 Hz), 3.81 (3H, d, J = 3.2 Hz), 6.85−6.92 (3H, m), 7.28−7.38 (3H,m), 7.93 (1H,dd, J = 2.8 Hz, 9 Hz), 9.28 (1H, d, J = 3.2 Hz). Anal. Calcd. for $C_{15}H_{14}N_2O_5$: C, 59.60; H, 4.67. Found: C, 60.25; H, 4.85.

***N*-(2-Hydroxy-5-nitrophenyl)-2-(4-methoxyphenyl)acetamide (7f) (AS-17).** From 2-amino-4-nitro-phenol (2.0 mmol, 308 mg), 4-methoxyphenylacetyl chloride (2.0 mmol, 370 mg), and pyridine (2.4 mmol, 189 mg), the general procedure for **3** gave **7e** as a yellow solid in quantitative yield. ^{1}H NMR (400 MHz, $CDCl_3$) δ 3.77 (2H, s), 3.78 (3H, s), 6.89 (2H, dd, J = 8.4 Hz), 7.26−7.29 (2H, m), 7.87 (1H, dd, J = 2.8 Hz, 9.2 Hz), 8.92 (1H, dd, J = 2.4 Hz), 9.48 (1H, s). Anal. Calcd for $C_{15}H_{14}N_2O_5$: C, 59.60; H, 4.67. Found: C, 60.08; H, 5.03.

***N*-(2-Hydroxy-5-nitrophenyl)-2-phenoxyacetamide (7g) (AS-18).** From 2-amino-4-nitro-phenol (2.0 mmol, 308 mg), phenoxyacetyl chloride (2.0 mmol, 342 mg), and pyridine (2.4 mmol, 190 mg), the general procedure for **3** gave **7g**, carried to the next step (hydrogenation) without further purification. ^{1}H NMR (400 MHz, $CDCl_3$) δ 4.81 (2H,s), 6.98−7.08 (3H, m), 7.26−7.31 (2H,m), 7.61 (1H,d, J = 9 Hz), 8.12 (1H,dd, J = 2.8 Hz, 9 Hz), 9.01 (1H,d, J = 2.8 Hz), 9.46 (1H,s), 10.13 (1H,s). Anal. Calcd for $C_{14}H_{12}N_2O_5$: C, 58.33; H, 4.20; N, 9.72. Found: C, 58.90; H, 4.36; N, 9.41.

***N*-(2-Hydroxy-4-nitrophenyl)-2-phenoxyacetamide (7h) (AS-9).** Phenoxyacetyl chloride (2.4 mmol, 410 mg) was added to a mixture of 2-amino-5-nitro-phenol (2 mmol, 308 mg) and potassium carbonate (2.4 mmol, 331 mg) in acetone (10 mL). The reaction mixture, which was changing color from red to light yellow, was stirred at room temperature for 2 h, poured into NH_4Cl (saturated aqueous), extracted with CH_2Cl_2 (3× 10 mL), and purified by recrystallization from CH_2Cl_2−hexane to obtain the compound as a light yellow solid. ^{1}H NMR (400 MHz, DMSO-d_6) δ 4.81 (2H,s), 6.98−7.03 (3H,m), 7.32−7.36 (2H,m), 7.692 (1H,d, J = 2.8 Hz), 7.77 (1H,dd, J = 2.4 Hz, 9.2 Hz), 8.38 (1H,d, J = 9.2 Hz), 9.53 (1H,s). Anal. Calcd for $C_{14}H_{12}N_2O_5$: C, 58.33; H, 4.20; N, 9.72. Found: C, 58.45; H, 4.28; N, 9.33.

3-(2-Phenylacetamido)-4-hydroxybenzamide (7i) (AS-111; Scheme 3). 4-Nitro-3-hydroxybenzoic acid (**7i-1**) (5 mmol, 916.0 mg) was added to a suspension of Me_3OBF_4 (5.5 mmol, 813.4 mg) in CH_2Cl_2 (20 mL) followed by diisopropylethylamine (5.5 mmol, 0.96 mL). During the addition of the amine, the reaction mixture spontaneously warmed, but once the process was completed, the suspension had dissolved to leave a clear yellow solution. The reaction was followed by TLC until the starting material was no longer detected. The mixture was purified by chromatography to achieve pure methylester **7i-2** (812 mg, 82% yield). The latter (1 mmol, 197 mg) was treated with concentrated ammonium hydroxide (37%, 4 mL) at 50−60 °C for 48 h. The reaction mixture was poured into water (10 mL), extracted with ethyl acetate (3× 6 mL), the organic layers combined, dried over Na_2SO_4, and then evaporated. The resulting solid was purified by chromatography to obtain amide **7i-3** as a yellow solid (56 mg, 31%).

Amide **7i-3** (6 mmol, 1.18 g) was dissolved in methanol and hydrogenated (45 psi (1 psi = 6.89 kPa)) for 3 h. The product **7i-4** was obtained after chromatography with methanol and ethyl acetate (1:9) as the eluant; 891 mg, 89% yield.

7i-4 (0.34 mmol, 51 mg) was treated with sodium hydride (0.4 mmol, 10 mg) in anhydrous THF(5 mL), followed by the addition of phenylacetyl chloride (0.38 mmol, 58 mg). The reaction mixture was stirred at room temperature for 5 h, until the starting material was no longer detected by TLC. The reaction solution was poured into H_2O, extracted with CH_3CN (2× 10 mL), and purified by chromatography to give **7i** as a white solid. ^{1}H NMR (400 MHz, DMSO-d_6) δ 3.78 (2H,s), 6.85 (1H,d, J = 8.4 Hz), 7.05−7.37 (5H,m), 7.48 (1H, dd, J = 2 Hz, 8.4 Hz), 8.24 (1H, J = 2 Hz), 9.42 (1H,s), 10.38 (1H, m). Anal. Calcd for $C_{15}H_{14}N_2O_3$: C, 66.66; H, 5.22. Found: C, 65.94; H, 5.04.

Methyl 3-(2-phenylacetamido)-4-hydroxybenzoate (7j) (AS-112). Methyl 3-amino-4-hydroxybenzoate (0.4 mmol, 67 mg) was treated with sodium hydride (0.48 mmol, 12 mg) in anhydrous THF-(5 mL), followed by the addition of phenylacetyl chloride (0.4 mmol, 62 mg). The reaction mixture was stirred at room temperature for 5 h, until starting the material was no longer detected by TLC, poured into H_2O, and extracted with ethyl acetate (10 mL). Purification by chromatography gave **7j** as a white solid. ^{1}HNMR (400 MHz, DMSO-d_6) δ 3.78 (2H, s), 3.79 (3H, s), 6.93 (1H, d, J = 8.4 Hz), 7.25−7.36 (m, 5H), 7.57 (1H, dd, J = 2.0 Hz, 8.4 Hz), 8.51 (1H, d, J = 2.0 Hz), 9.42 (1H, s). Anal. Calcd for $C_{16}H_{15}NO_4$: C, 67.36; H, 5.30; N, 4.91. Found: C, 66.72; H, 5.31; N, 4.84.

***N*-(5-(Trifluoromethyl)-2-hydroxyphenyl)-2-phenylacetamide (7k) (AS-130).** 2-Nitro-4-(trifluoromethyl)phenol (4.83 mmol, 1 g) was hydrogenated in methanol, filtered, and evaporated to give crude product 488 mg, which was carried to the next step without further purification. From crude 2-amino-4-(trifluoromethyl)phenol (2.76 mmol, 488 mg,), phenylacetyl chloride (2.76 mmol, 425 mg), and pyridine (3.31 mmol, 262 mg), the general procedure for **3** gave **7k** as a white solid in quantitative yield. ^{1}H NMR (400 MHz, DMSO-d_6) δ 3.82 (2H, s), 7.05 (2H, m), 7.34−7.46 (7H, m), 9.17 (1H, s). Anal. Calcd for $C_{15}H_{12}F_3NO_2$: C, 61.02; H, 4.10; N, 4.74. Found: C, 60.87; H, 4.05; N, 4.72.

Synthesis of Compound 8. $LiAlH_4$ (1.0 M/THF, 10 mmol) was added dropwise to a solution of anthranilic acid (4 mmol, 809 mg) in anhydrous THF (10 mL) at 0 °C. After stirring for 2 h at room temperature, the reaction mixture was heated to reflux for an additional 15 min, then cooled in an ice bath. The mixed solvent of THF and H_2O was added carefully to the reaction mixture until bubbles were no longer evident. The resulting white precipitate was filtered off and the filtrate concentrated and purified by chromatography to provide **8a** as a light brown solid in 21% yield. ^{1}H

NMR (600 MHz, $CDCl_3$) δ 4.58 (2H, br), 4.79 (2H, s), 7.20 (1H, d, $J = 7.8$ Hz), 7.51 (1H, d, $J = 1.8$ Hz), 7.54 (1H, dd, $J = 1.8$ Hz, 7.8 Hz).

Compound 8b. Compound **8a** (70 mg, 0.42 mmol) was added to a suspension of sodium hydride (12 mg, 0.46 mmol) in THF (1 mL) at 0 °C. The reaction mixture was stirred at 0 °C for 15 min, and then TBDMSCl (1.0 M/THF, 0.504 mmol, 0.504 mL) was added dropwise. The reaction was warmed to room temperature and stirred at this temperature for another 3 h until the starting material was no longer detected by TLC. The reaction mixture was poured into brine (5 mL) and extracted with EtOAc (3× 5 mL). **8b** was used in the next step for the synthesis of compound **8c** without further purification.

Compound **8c** was obtained as a yellow solid in 43% yield using the general procedure for the synthesis of **3**. ^{1}H NMR (600 MHz, $CDCl_3$) δ 0.11 (9H, s), 1.22 (6H, s), 3.78 (2H, s), 4.61 (2H, s), 7.24−7.40 (5H, m), 7.88 (1H, dd, $J = 1.8$ Hz, 8.1 Hz), 8.77 (1H, s), 9.08 (1H, d, $J = 1.8$ Hz).

Hydrogenation of Compound 8c. The hydrogenation of **8c** following the general procedure delivered **8d** in quantitative yield. ^{1}H NMR (400 MHz, $CDCl_3$) δ 0.01 (6H, s), 0.85 (9H, s), 3.68 (2H, s), 4.49 (2H, s), 6.31 (1H, dd, $J = 2.0$ Hz, 7.8 Hz), 6.82 (1H, d, $J = 8.0$ Hz), 7.28−7.36 (5H, m), 7.63 (1H, d, $J = 2.4$ Hz), 8.70 (1H, br).

Deprotection of 8d. Compound **8d** (24 mg, 0.065 mmol) was treated with TBAF (1.0 M/THF, 0.195 mmol) in THF (2 mL). The reaction mixture was poured into brine (5 mL), and upon disappearance of all starting material (TLC), extracted by EtOAc, dried over anhydrous $MgSO_4$, and purified by chromatography to give **8** as a white solid in quantitative yield. ^{1}H NMR (600 MHz, $CDCl_3$) δ 3.68 (2H, s), 4.35 (2H, s), 6.29 (1H, dd, $J = 1.8$ Hz, 7.8 Hz), 6.83 (1H, d, $J = 8.4$ Hz), 7.31−7.39 (5H, m), 7.49 (1H, d, $J = 1.8$ Hz), 8.41 (1H, s).

Synthesis of Compound 9. A solution of **11k** (0.3 mmol, 85.9 mg) and Pd/C powder (8.5 mg) in methanol (10 mL) under hydrogen (50 psi) was shaken for 2.5 h. The Pd/C was removed by filtering through a Celite cake, and methanol was removed under reduced pressure. The resulting residue was purified by column chromatography (10:1 DCM/ethanol) providing **9** as a white solid (73.0 mg, yield 95%): R_f =0.27 (10:1, DCM/ethanol). ^{1}H NMR (400 MHz, DMSO-d_6) δ 9.81 (1H, s), 7.21−7.32 (5H, m), 6.80 (1H, s), 6.65 (1H, s), 6.22 (1H, s), 5.01 (2H, br), 4.98 (1H, t, $J =$ 5.6 Hz), 4.28 (2H, d, $J = 5.6$ Hz), 3.57 (2H, s); ^{13}C NMR (100 MHz,DMSO-d_6) δ 168.67, 148.77, 143.45, 139.57, 136.37, 129.00, 128.28, 126.45, 107.41, 105.42, 103.38, 63.18, 43.47. Anal. Calcd for $C_{15}H_{17}N_2O_2\cdot 0.3\ H_2O$: C, 68.84; H, 6.39; N, 10.70. Found: C, 68.56; H, 6.30; N, 10.59.

***N*-(4-Hydroxy-3-nitrophenyl)-2-phenylacetamide (11a) (AS-13).** From 2-nitro-4-amino-phenol (2 mmol, 308 mg), phenylacetyl chloride (2 mmol, 308 mg), and pyridine (2.4 mmol, 190 mg), the general procedure for **3** delivered **11a** as a yellow solid in quantitative yield.^{1}H NMR (600 MHz, $CDCl_3$) δ 3.79 (2H,s), 7.08-(1H, br), 7.09 (1H, d, $J = 9.3$ Hz), 7.26−7.44 (5H, m), 7.67 (1H, dd, $J = 2.4$ Hz, 9.3 Hz), 8.17 (1H, d, $J = 2.4$ Hz), 10.40 (1H, s). Anal. Calcd for $C_{14}H_{12}N_2O_4$: C, 61.76; H, 4.44; N, 10.29. Found: C, 62.09; H, 4.46; N, 10.10.

***N*-(4-Fluoro-3-nitrophenyl)-2-phenylacetamide (11b) (RK-3).** From 4-fluoro-2-nitro-aniline (2 mmol, 308 mg), phenylacetyl chloride (2 mmol, 308 mg), and pyridine (2.4 mmol, 190 mg), the general procedure for **3** gave **11b** as a yellow solid in quantitative yield. ^{1}H NMR (400 MHz, $CDCl_3$) δ 3.79 (2H, s), 7.21 (1H, dd, J = 9.2 Hz, 10.4 Hz), 7.33−7.46 (5H, m), 7.77−7.81 (1H, m), 8.09 (1H, dd, $J = 2.4$ Hz, 6.6 Hz). Anal. Calcd for $C_{14}H_{11}FN_2O_3$: C, 61.31; H, 4.04; N, 10.21. Found: C, 61.32; H, 4.04; N, 10.15.

***N*-(3,5-Dinitro-phenyl)-2-phenyl-acetamide (11c).** From 3,5-dinitro-aniline (1 mmol, 183 mg), phenylacetyl chloride (1 mmol, 155 mg), and pyridine (1.1 mmol, 87 mg), the general procedure for **3** gave **11c** in 85% yield as a light yellow solid. ^{1}H NMR (400 MHz, $CDCl_3$) δ 3.84 (2H, s), 7.35−7.49(6H, m), 8.68 (2H, d, $J =$ 2.0 Hz), 8.74 (1H, dd, $J = 2.0$ Hz, 1.8 Hz). Anal. Calcd for $C_{14}H_{11}N_3O_5$: C, 55.82; H, 3.68; N 13.95. Found: C, 55.83; H, 3.64; N, 14.03.

2-(2-Phenylacetamido)-4-nitrophenyl 2-phenylacetate (11d) (NL-11). From 2-amino-4-nitro-phenol, the general procedure for **3** gave **11d** as a byproduct of the synthesis of **7d**. ^{1}H NMR (400 MHz, $CDCl_3$) δ 3.59(2H, s), 3.62 (2H, s), 7.26−7.48 (10H, m), 7.99 (1H, d, $J = 2.8$ Hz), 8.09 (1H, dd, $J = 2.4$ Hz, 9.2 Hz), 8.62 (1H, d, $J = 9.2$ Hz). Anal. Calcd for $C_{22}H_{18}N_2O_5$:C, 67.69; H, 4.65; N, 7.18. Found: C, 66.86; H, 4.55; N, 7.60.

***N*-(3-Amino-5-nitrophenyl)-2-phenylacetamide (11e)** In a 50 mL three necked round-bottomed flask equipped with a reflux condenser and a stirrer, a mixture of *N*-(3,5-dinitrophenyl)-2-phenylacetamide (150.5 mg, 0.50 mmol), 5.5 mg 10% palladium on carbon, and triethylamine (0.31 mL, 2.25 mmol) in 2 mL of acetonitrile was heated to reflux. A solution of 98% formic acid (0.08 mL, 2.15 mmol) in 0.5 mL of acetonitrile was carefully added dropwise over 10 min. The mixture was refluxed for 1−1.5 h. The reduction progress was followed by TLC (1:1, Hexane/Ethyl acetate) and the reaction terminated after the disappearance of the starting material. Upon cooling, the reaction mixture was filtered to remove the catalyst and extracted with ethyl acetate. The combined organic phases were washed with saturated aqueous $NH_3\cdot$HCl, dried over anhydrous $MgSO_4$, filtered, and concentrated under reduced pressure. The residue was purified by silica gel chromatography (1:1, hexane/ethyl acetate), providing **11e** (59.8 mg, 55%) as a yellow solid: R_f =0.40 (1:1, hexane/ethyl acetate). ^{1}H NMR (400 MHz, DMSO-d_6) δ 10.31 (1H, s), 7.65 (1H, t, $J = 2.0$ Hz), 7.32−7.33 (4H, m), 7.24−7.27 (1H, m), 7.22 (1H, d, $J = 2.0$ Hz), 7.08 (1H, t, $J = 2.0$ Hz), 5.85 (2H, s), 3.63 (2H, s); ^{13}C NMR (100 MHz,DMSO-d_6) δ 169.54, 148.80, 140.55, 135.74, 129.09, 128.34, 126.63, 109.35, 102.62, 100.95, 43.38; IR. Anal. Calcd for $C_{14}H_{13}N_3O_3$:C, 61.99; H, 4.83; N, 15.49. Found: C, 61.50; H, 4.80; N, 15.29.

4-Nitro-2-phenylacetylamino-benzamide (11f). (AS-48) 4-Nitroanthranilic acid (**12a**) (182 mg, 1.0 mmol) in thionyl chloride (10 mL) was heated at 60 °C for 3 h under N_2 and concentrated by rotary evaporation. The $SOCl_2$ residue was removed by addition of CH_2Cl_2. Concentrated aqueous NH_3 (10 mL) was then added, and the mixture was stirred overnight at room temperature. The precipitates formed were collected by filtration and washed with water several times, and the filtrate was extracted with ethyl acetate (3× 5 mL). The combined crude product was purified by recrystallization (MeOH) to afford pure **13a** in two steps in 27% yield. Compound **13a** was further treated with phenyl acetyl chloride to give the desired compound **11f** as a light yellow solid in 67% yield. ^{1}H NMR (600 MHz, $CDCl_3$) δ 3.79 (2H, s), 7.33−7.41(5H, m), 7.62 (1H, d, $J = 8.4$ Hz), 7.88 (1H, dd, $J = 2.4$ Hz, 8.4 Hz), 9.55 (1H, d, $J = 1.8$ Hz), 11.08 (1H, s). ^{13}C NMR (100 MHz, $CDCl_3$) δ 170.93, 141.71, 130.25, 129.71, 128.77, 128.29, 117.74, 117.14, 46.52. Anal. Calcd for $C_{15}H_{13}N_3O_4$: C, 60.20; H, 4.38; N 14.04. Found: C, 60.29; H, 4.50; N, 13.27.

3-(2-Phenylacetylamino)-5-nitrobenzamide (11g). Using the same procedure as that used for the preparation of **11f**, **11g** was obtained as a yellow solid in 80% yield. ^{1}H NMR (400 MHz, DMSO-d_6) δ 3.76 (2H, s), 7.24−7.36 (5H, m), 7.67 (1H, s), 8.34 (1H, s), 8.40 (2H, dd, $J = 1.4$ Hz, 4.8 Hz), 8.77 (1H, t, $J = 2.0$ Hz), 10.80 (1H,s). Anal. Calcd for $C_{15}H_{13}N_3O_4$: C, 60.20; H, 4.38; N 14.04. Found: C, 60.45; H, 4.34; N, 13.63.

***N*-(3-(hydroxyamino)-5-nitrophenyl-2-phenylacetamide (11h).** A mixture of *N*-(3,5-dinitrophenyl)-2-phenylacetamide (150.5 mg, 0.5 mmol) and anhydrous hydrazine (0.05 mL, 1.5 mmol) in 1:1 v/v ethanol/dichloroethane (1.5 mL) was stirred for 10 min at room temperature, followed by the addition of Raney nickel (1.5 mg). The reaction is vigorous, and the temperature increased to 50−60 °C. (The temperature was not allowed to rise above 60 °C.) After 30 min, when the reaction had subsided, stirring was continued for 4 h at 50−60 °C. The mixture was then filtered to remove the catalyst and extracted with ethyl acetate. The combined organic phases were washed with saturated aqueous $NH_3\cdot$HCl, dried over anhydrous $MgSO_4$, filtered, and concentrated under reduced pressure. The residue was purified by silica gel chromatography (1:1,

hexane/ethyl acetate), providing **11h** (72.0 mg, 50%) as a yellow solid: R_f =0.40 (1:1, hexane/ethyl acetate). ^{1}H NMR (400 MHz, DMSO-d_6) δ 10.50 (1H, s), 8.89 (1H, s), 8.74 (1H, d, J = 1.6 Hz), 7.97 (1H, t, J = 2.0 Hz), 7.47 (1H, t, J = 2.0 Hz), 7.33−7.34 (4H, m), 7.29 (1H, t, J = 2 Hz), 7.24−7.27 (1H, m), 3.65 (2H, s); ^{13}C NMR (100 MHz,DMSO-d_6) δ 169.72, 153.51, 148.47, 140.41, 135.60, 129.12, 128.37, 126.66, 108.20, 104.04, 101.56, 43.39. Anal. Calcd for $C_{14}H_{13}N_3O_4$: C, 58.53; H, 4.56; N, 14.63. Found: C, 58.71; H, 4.68; N, 14.45.

Methyl 3-(2-phenylacetamido)-5-nitrobenzoate (11i). The procedure is similar to the synthesis of **3.** ^{1}H NMR (400 MHz, $CDCl_3$) δ 8.70 (1H, t, J = 2.4 Hz), 8.56 (1H, t, J = 1.6 Hz), 8.28 (1H, t, J = 1.8 Hz), 7.50 (1H, br), 7.34−7.47 (5H, m), 3.96 (3H, s), 3.82 (2H, s); ^{13}C NMR (100 MHz, $CDCl_3$) δ 170.15, 164.90, 148.74, 139.35, 133.69, 132.31, 129.63, 129.53, 128.16, 126.07, 119.95, 118.55, 53.10, 44.72. Anal. Calcd for $C_{16}H_{14}N_2O_5$: C, 61.14; H, 4.49; N, 8.91. Found: C, 61.41; H, 4.40; N, 8.80.

3-(2-Phenylacetamido)-5-nitrobenzoic Acid (11j). A mixture of **11i** (0.40 mmol, 125 mg) and lithium hydroxide (1.4 mmol, 60.0 mg) in MeOH (15 mL) and H_2O (5 mL) was stirred for 4 h at room temperature. The resulting mixture was extracted with ethyl acetate, and the combined organic phases were washed with saturated aqueous NH_3·HCl, dried over anhydrous $MgSO_4$, filtered, and concentrated under reduced pressure. The residue was purified by silica gel chromatography (4:1, ethyl acetate/ethanol) providing **11j** (114.3 mg, 96%) as a pale yellow solid: R_f =0.32 (4:1, ethyl acetate/ethanol). ^{1}H NMR (400 MHz, DMSO-d_6) δ 11.03 (1H, s), 8.79 (1H, s), 8.57 (1H, s), 8.37 (1H, s), 7.23−7.39 (5H, m), 3.73 (2H, s); ^{13}C NMR (100 MHz,DMSO-d_6) δ 170.09, 167.34, 147.66, 140.75, 139.95, 135.77, 129.22, 128.36, 126.65, 126.21, 118.22, 113.97, 43.31. Anal. Calcd for $C_{15}H_{12}N_2O_5.0.4CH_2Cl_2$:C, 55.66; H, 3.86; N, 8.49. Found: C, 55.36; H, 3.68; N, 8.52.

***N*-(3-(Hydroxymethyl)-5-nitrophenyl)-2-phenylacetamide (11k).** A solution of **11i** (1.5 mmol, 471.0 mg) in MeOH (10 mL) was slowly added dropwise to a solution of sodium borohydride (10.0 mmol, 378.3 mg) in MeOH (10 mL). The resulting mixture was refluxed for 4 h, quenched by H_2O, and extracted with ethyl acetate. The combined organic phases were washed with brine, dried over anhydrous $MgSO_4$, filtered, and concentrated under reduced pressure. The residue was purified by silica gel chromatography (1:1, ethyl acetate/hexane) providing **11k** (86.8 mg, 20%) as a yellow solid: R_f =0.37 (1:1, ethyl acetate/hexane). ^{1}H NMR (400 MHz, DMSO-d_6) δ 10.66 (1H, s), 8.51 (1H, t, J = 2.0 Hz), 7.89 (1H, s), 7.84(1H, s), 7.23−7.36 (5H, m), 5.55 (1H, t, J = 5.6 Hz), 4.58 (2H, d, J = 5.6 Hz), 3.68 (2H, s); ^{13}C NMR (100 MHz,DMSO-d_6) δ 169.89, 147.92, 145.57, 140.10, 135.51, 129.16, 128.38, 126.71, 122.41, 115.19, 111.51, 61.85, 43.35. Anal. Calcd for $C_{15}H_{14}N_2O_4$: C, 62.93; H, 4.93; N, 9.79. Found: C, 62.69; H, 4.96; N, 9.72.

3-(2-Phenylacetamido)-5-aminobenzamide (14a). 11g (0.37 mmol, 109 mg) was dissolved in methanol, hydrogenated (50 psi (1 psi = 6.89 kPa)), and the combined filtrates washed with methanol. The product **14a** was purified by chromatography with methanol and ethyl acetate (1:9) as eluants; 78 mg, 80% yield. ^{1}H NMR (400 MHz, DMSO-d_6) δ 3.60 (2H, s), 5.21 (2H, s), 6.67 (1H, s), 7.06 (2H, s), 7.21−7.33 (5H, m), 7.64(1H, s), 9.97(1H, s). HRMS calcd for $C_{15}H_{15}N_3O_2$ 269.11643; found, 270.12357 $[M + H]^+$.

3-(2-Phenylacetoyloxy)-5-aminobenzoic acid (14b). The procedure is similar to that used for **11j** and gave **14b** as a white solid: R_f =0.60 (4:1, ethyl acetate/ ethanol). ^{1}H NMR (600 MHz, DMSO-d_6) δ 10.13 (1H, s), 7.30−7.32 (4H, m), 7.28 (1H, s), 7.22−7.25 (1H, m), 7.13 (1H, s), 6.86 (1H, s), 5.30 (2H, s), 3.59 (2H, s); ^{13}C NMR (150 MHz,DMSO-d_6) δ 168.96, 168.33, 149.07, 139.72, 136.20, 132.58, 129.05, 128.30, 126.50, 110.05, 108.18, 43.42. Anal. Calcd for $C_{15}H_{14}N_2O_3.1.1H_2O$: C, 62.10; H, 5.63; N, 9.66. Found: C, 62.15; H, 5.15; N, 9.13.

***N*-(3,5-diaminophenyl)-2-phenylacetamide (14c). 11c** was dissolved in methanol. Hydrogenation provided **14c** as a light pink solid in quantitative yield. ^{1}H NMR (400 MHz, DMSO-d_6) δ 3.58 (2H, s), 4.65 (4H, s), 5.55 (1H,t, J = 1.8 Hz), 6.10 (2H,d, J = 2.0 Hz), 7.19−7.27 (5H, m), 9.55 (1H, s). HRMS calcd for $C_{14}H_{15}N_3O$ 241.1215; found, 242.1288 $[M + H]^+$.

2-(2-Fluorophenyl)-*N*-(3-nitrophenyl)acetamide (15a). The procedure is similar to that used for **15b**. **15a** was obtained as a pale yellow solid (504.7 mg, 92%). ^{1}H NMR (400 MHz, DMSO-d_6) δ 10.72 (1H, s), 8.63 (1H, t, J = 2.0 Hz), 7.91 (2H, dd, J_1 = 8.4 Hz, J_2 = 2.0 Hz), 7.61 (1H, t, J = 8.4 Hz), 7.41 (1H, dt, J_1 = 7.6 Hz, J_2 = 1.6 Hz), 7.30−7.36 (1H, m), 7.15−7.21 (2H, m), 3.79 (2H, s); ^{13}C NMR (100 MHz, DMSO-d_6) δ 168.87, 160.69 (d, J = 242.8 Hz), 147.97, 140.21, 132.07 (d, J = 3.8 Hz), 130.25, 128.99 (d, J = 7.6 Hz), 125.02, 124.29 (d, J = 3.0 Hz), 122.45 (d, J = 16.0 Hz), 117.81, 115.06 (d, J = 21.2 Hz), 113.16, 36.38. Anal. Calcd for $C_{14}H_{11}FN_2O_3$: C, 61.31; H, 4.04; N, 10.21. Found: C, 61.30; H, 3.95; N, 10.13.

2-(2-Iodophenyl)-*N*-(3-nitrophenyl)acetamide (15b). In a 50 mL three necked round-bottom flask equipped with a reflux condenser and a stirrer, 2-iodophenylacetic acid (262.0 mg, 1.0 mmol) was dissolved in thionyl chloride (20 mL) at room temperature, and the resulting solution was stirred for 2 h at reflux. The thionyl chloride excess was removed under reduced pressure. The residue was dissolved in THF (10 mL) at room temperature, and 3-nitroaniline (138.1 mg, 1.0 mmol) and pyridine (0.097 mL, 1.2 mmol) were added consecutively. After stirring at room temperature for 2.5 h, the resulting mixture was quenched with saturated aqueous $NaHCO_3$ (10 mL), and the product was extracted with ethyl acetate (3× 20 mL). The combined organic phases were washed with brine, dried over anhydrous $MgSO_4$, filtered, and concentrated under reduced pressure. The crude product was purified by recrystallization in CH_2Cl_2 to give **15b** as a pale yellow solid (351.5 mg, 92%): R_f =0.45 (1:1, hexane/ethyl acetate). ^{1}H NMR (400 MHz, DMSO-d_6) δ 10.76 (1H, s), 8.64 (1H, t, J = 2.0 Hz), 7.92 (2H, d, J = 8.4 Hz), 7.86 (1H, d, J = 7.6 Hz), 7.62 (1H, t, J = 8.4 Hz), 7.36−7.41 (2H, m), 7.01−7.06 (1H, m), 3.90 (2H, s); ^{13}C NMR (150 MHz,DMSO-d_6) δ 168.77, 147.99, 140.30, 138.84, 138.73, 131.48, 130.29, 128.87, 128.28, 124.97, 117.75, 113.08, 101.81, 47.67. Anal. Calcd for $C_{14}H_{11}IN_2O_3$: C, 44.00; H, 2.90; N, 7.33. Found: C, 44.29; H, 2.89; N, 7.28.

2-(3-Fluorophenyl)-*N*-(3-nitrophenyl)acetamide (16a). The procedure is similar to that used for **15b**; pale white solid (509.6 mg, 93.0%). ^{1}H NMR (400 MHz, DMSO-d_6) δ 10.69 (1H, s), 8.62 (1H, t, J = 2.0 Hz), 7.90−7.93 (2H, dm, J = 8.4 Hz), 7.61 (1H, t, J = 8.4 Hz), 7.35−7.41 (1H, m), 7.17−7.20 (2H, m), 7.08−7.13 (1H, tm, J_1 = 8.4 Hz), 3.74 (2H, s); ^{13}C NMR (100 MHz, DMSO-d_6) δ 169.37, 162.06 (d, J = 242.1 Hz), 147.94, 140.18, 138.09 (d, J = 7.6 Hz), 130.23, 130.18 (d, J = 8.4 Hz), 125.43 (d, J = 2.2 Hz), 125.07, 117.85, 116.10 (d, J = 21.2 Hz), 113.52 (d, J = 20.5 Hz), 113.21, 42.73. Anal. Calcd for $C_{14}H_{11}FN_2O_3$:C, 61.31; H, 4.04; N, 10.21. Found: C, 61.24; H, 4.05; N, 10.09.

2-(3-Iodophenyl)-*N*-(3-nitrophenyl)acetamide (16b). The procedure is similar to that in **15b**; pale yellow solid (363.0 mg, 95%): R_f =0.63 (1:1, hexane/ethyl acetate). ^{1}H NMR (400 MHz, DMSO-d_6) δ 10.68 (1H, s), 8.62 (1H, t, J = 2.0 Hz), 7.91 (2H, dd, J = 8.0 Hz, J_2= 2.0 Hz), 7.74 (1H, s), 7.58−7.64 (2H, m), 7.36 (2H, d, J = 7.6 Hz), 7.15 (1H, t, J = 7.6 Hz), 3.68 (2H, s); ^{13}C NMR (150 MHz,DMSO-d_6) δ 169.44, 147.96, 140.16, 138.00, 137.87, 135.44, 130.53, 130.26, 128.78, 125.07, 117.88, 113.19, 94.77, 42.47. Anal. Calcd for $C_{14}H_{11}IN_2O_3$: C, 44.00; H, 2.90; N, 7.33. Found: C, 44.24; H, 2.87; N, 7.40.

2-(4-Fluorophenyl)-*N*-(3-nitrophenyl)acetamide (17a). The procedure is similar to that used for **15b**; pale white solid (516.7 mg, 94.2%). ^{1}H NMR (400 MHz, DMSO-d_6) δ 10.67 (1H, s), 8.62 (1H, t, J = 2.0 Hz), 7.91 (2H, dm, J = 8.4 Hz), 7.60 (1H, t, J = 8.4 Hz), 7.37 (2H, m), 7.16 (2H, tt, J_1 = 9.2 Hz, J_2 = 2.4 Hz), 3.70 (2Hs, s); ^{13}C NMR (100 MHz,DMSO-d_6) δ 169.82, 161.19 (d, J = 240.5 Hz), 147.94, 140.24, 131.58 (d, J = 3.0 Hz), 131.11 (d, J = 8.3 Hz), 130.23, 125.04, 117.80, 115.07 (d, J = 21.3 Hz), 113.17, 42.23. Anal. Calcd for $C_{14}H_{11}FN_2O_3$: C, 61.31; H, 4.04; N, 10.21. Found: C, 61.06; H, 3.96; N, 10.03.

2-(4-Iodophenyl)-*N*-(3-nitrophenyl)acetamide (17b). The procedure is similar to that used for **15b**; pale white solid (363.0 mg, 95%). ^{1}H NMR (400 MHz, DMSO-d_6) δ 10.67 (1H, s), 8.61 (1H,

t, $J = 2.0$ Hz), 7.90 (2H, dd, $J_1 = 8.0$ Hz, $J_2 = 2.0$ Hz), 7.69 (2H, dt, $J = 8.4$ Hz, $J_2 = 2.0$ Hz), 7.60 (1H, t, $J = 8.4$ Hz), 7.15 (2H, t, $J = 8.0$ Hz), 3.67 (2H, s); ^{13}C NMR (150 MHz,DMSO-d_6) δ 169.44, 147.94, 140.12, 137.10, 135.21, 131.68, 130.25, 125.01, 117.85, 113.15, 92.66, 42.61. Anal. Calcd for $C_{14}H_{11}IN_2O_3$: C, 44.00; H, 2.90; N, 7.33. Found: C, 43.86; H, 2.86; N, 7.34.

General Procedure for the Synthesis of Nitrophenyl Pyridinyl Acetamides (18−20). Triethylamine (1.13 mmol, 160 uL) was added to pyridyl acetic acid hydrochloride (200 mg, 1.13 mmol) in CH_2Cl_2 (5 mL) at room temperature. The reaction mixture immediately turned red, to which dimethylaminopropyl-3-ethyl-carbodiimide hydrochloride (EDCI) (250 mg, 1.1 equiv, 1.24 mmol) was added, followed by the addition of DMAP (15 mg) and stirring for 15 min. Nitro aniline was added to the above reaction mixture, which was stirred for 24 h at 0 °C. The reaction solution was poured into $NaHCO_3$ (sat. 5 mL) and extracted with EtOAc (3× 10 mL). The combined the organic layers were dried over $MgSO_4$, evaporated, and washed with cold chloroform to afford a yellow powder.

***N*-(3-Nitrophenyl)-2-(pyridin-2-yl)acetamide (18).** The product was obtained in 40.5% yield. ^{1}H NMR (300 MHz, $CDCl_3$) δ 3.94 (2H, s), 7.34 (2H, m), 7.48 (1H, t, $J = 8.4$ Hz), 7.76 (1H, t, $J = 7.5$ Hz, 1H), 7.93 (1H, d, $J = 7.5$ Hz), 8.01 (1H, d, $J = 8.0$ Hz), 8.40 (1H, t, $J = 2.3$ Hz), 8.65 (1H, d, $J = 5.1$ Hz), 10.60 (1H, bs); ^{13}C NMR (100 MHz, $CDCl_3$) δ 45.37, 114.63, 1118.63, 122.76, 124.70, 125.64, 129.80, 137.97, 139.46, 148.61, 148.96, 154.92. 167.86; HRMS calcd for $C_{13}H_{11}N_3O_3$: 257.08004; found 258.08716 $[M + H]^+$. Anal. Calcd for $C_{13}H_{11}N_3O_3$: C, 60.70; H, 4.31; N, 16.33. Found: C, 60.74; H, 4.35; N, 16.09.

***N*-(3-Nitrophenyl)-2-(pyridin-3-yl)acetamide (19).** The product was furnished in 28% yield. ^{1}H NMR (600 MHz, DMSO-d_6) δ 3.77 (2H, s), 7.37 (1H, dd, $J = 4.8$ Hz, 7.2 Hz), 7.61 (1H, t, $J = 1.8$ Hz), 7.75 (1H, d, $J = 7.8$ Hz), 7.91 (2H, dd, $J = 2$ Hz, 8.1 Hz), 8.47 (1H, dd, $J = 1.8$, 4.8), 8.53 (1H, d, $J = 1.8$ Hz), 8.62 (1H, t, $J = 2$ Hz) ^{13}C NMR (150 MHz, DMSO-d_6) δ 40.10, 113.24, 117.91, 123.46, 125.11, 130.27, 131.13, 136.93, 140.15, 147.98, 150.29, 169.39. HRMS calcd for $C_{13}H_{11}N_3O_3$ 257.08004; found, 258.08715 $[M + H]^+$. Anal. Calcd for $C_{13}H_{11}N_3O_3$: C, 60.70; H, 4.31; N, 16.33. Found: C, 59.54; H, 4.33; N, 15.92.

***N*-(3-Nitrophenyl)-2-(pyridin-4-yl)acetamide (20).** The product was obtained in 51% yield. ^{1}H NMR (400 MHz, DMSO-d_6) δ 3.76 (2H, s), 7.36 (2H, d, $J = 6.0$ Hz), 7.61(1H, t, $J = 8.2$ Hz), 7.92 (2H, m), 8.52 (2H, d, $J = 6.0$ Hz), 8.62 (1H, t, $J = 2.2$ Hz); ^{13}C NMR (100 MHz, DMSO-d_6) δ 41.97, 112.90, 117.63, 124.40, 124.77, 129.94, 139.72, 143.82, 147.61, 149.20, 151.93, 168.32. HRMS calcd for $C_{13}H_{11}N_3O_3$ 257.08004; found, 258.08715 $[M + H]^+$. Anal. Calcd for $C_{13}H_{11}N_3O_3$: C, 60.70; H, 4.31; N, 16.33. Found: C, 60.83; H, 4.36; N, 16.16.

Synthesis of Compound 21. From 2-amino-4-nitrophenol (2 mmol, 308 mg), benzylsulfonyl chloride (2 mmol, 382 mg), and pyridine (2.4 mmol, 2.4 mL), the general procedure for **3** gave **21** as shining yellow crystals in 65% yield. ^{1}H NMR (400 MHz,$CDCl_3$) δ 4.62 (2H, s), 6.91 (1H, d, $J = 8.8$ Hz), 7.46−7.51 (6H, m), 7.57 (1H, d, $J = 2.4$ Hz). Anal. Calcd for $C_{14}H_{15}N_2O_5S$: C, 50.64; H, 3.92; N, 9.09. Found: C, 50.70; H, 3.88; N, 9.00.

Computational Methods. Homology Model SAR. Low energy conformations of the ligands were derived by Monte Carlo conformational searching using the MMFF force field[42−44] in Macromodel v6.5 (Schrödinger, Inc., New York, NY) and a 7 kcal/mol energy cutoff window. Ligand conformations were manually docked into the cylindrical MV fusion-protein pocket occupied by Val94 using the assistance of Sybyl's DOCK, a manual docking algorithm, and visualization of the protein as its Connolly surface (Sybyl7.0, Tripos Discovery Software, St. Louis).[45,46] All complexes were relieved of short steric contacts with low-temperature molecular dynamics (20 K, TVN ensemble; 3−5 ps, Tripos force field) followed by active site minimization (Powell gradient,[47] convergence threshold of 0.05 kcal/(mol·Å), Tripos force field). Regions of the protein greater than 12 Å away from the ligand were held fixed to prevent the unfolding of the protein in the absence of explicit solvation.

QSAR via Molecular Field Topology Analysis (MFTA). MFTAWin software was used to analyze the effect of the local molecular properties on activity. First, the topological alignment of the training set structures and construction of a molecular supergraph that provides a common reference framework for a uniform descriptor set was carried out. In the next step, the PLS (partial least squares) regression model was built. Predictivity was assessed by means of a cross-validation procedure. Unlike the more widely employed leave-one-out scheme, the data set of 29 MV inhibitors (**3a**−**3g**, **4a**, **4b**, **7b**, **7d**−**7f**, **7i**−**7k**, **11a**−**11k**, **14a**−**14c**; Tables 1−3) in our computations was divided into four subsets of roughly the same size (leave-25%-out cross-validation). Then the data from three of the subsets (75% of the compounds) was used to construct a model, and one subset (25% of the compounds) was used for predictions. By repeating this procedure four times, a rather reliable estimate of q^2 cross-validation parameter was calculated, characterizing the average error of prediction in comparison to the model fit error. From 10 potential models, we selected as representative of the data a model with a good q^2 value, which included a reasonable number of descriptor types. In the present case, these are atomic charge (Q), H-bonding (H_a and H_d), and lipophilicity (L_g). Then the selected descriptor set was used to construct the PLS model for the whole 29-compound dataset. The fitting diagram for this model is shown in Figure 7.

Acknowledgment. This work was supported in part by grants from the American Lung Association and Public Health Service grant A1056179 and A1071002 from NIH/NIAID (to R.K.P. and J.P.S.).

Supporting Information Available: MFTA test set validation, dose response curves, table of elemental analyses, and additional synthetic procedures. This material is available free of charge via the Internet at http://pubs.acs.org.

References

(1) Lamb, R. A.; Kolakosky, D. Paramyxoviruses: The viruses and their replication. In *Fundamental Virology;* Fields, B. N., Knipe, D. M., Howley, P. M. Eds.; Lippencott-Raven: Philadelphia, PA, 1996; pp 577−604.
(2) Hilleman, M. R. Current overview of the pathogenesis and prophylaxis of measles with focus on practical implications. *Vaccine* **2001**, *20*, 651−665.
(3) CDC. Progress in reducing measles mortality−worldwide, 1999−2003. *MMWR* **2005**, *54*, 200−203.
(4) Gans, H. A.; Arvin, A. M.; Galinus, J.; Logan, L.; DeHovitz, R.; Maldonado, Y. Deficiency of the humoral immune response to measles vaccine in infants immunized at age 6 months. *JAMA* **1998**, *280*, 527−532.
(5) Polack, F. P.; Lee, S. H.; Permar, S.; Manyara, E.; Nousari, H. G.; Jeng, Y.; Mustafa, F.; Valsamakis, A.; Adams, R. J.; Robinson, H. L.; Griffin, D. E. Successful DNA immunization against measles: neutralizing antibody against either the hemagglutinin or fusion glycoprotein protects rhesus macaques without evidence of atypical measles. *Nat. Med.* **2000**, *6*, 776−781.
(6) In November 2005, the media reported an outbreak of over 2500 infections and eight deaths in Romania resulting from the government's failure to provide full vaccine coverage for children.
(7) Jansen, V. A.; Stollenwerk, N.; Jensen, H. J.; Ramsay, M. E.; Edmunds, W. J.; Rhodes, C. J. Measles outbreaks in a population with declining vaccine uptake. *Science* **2003**, *301*, 804.
(8) Mossong, J.; Nokes, D. J.; Edmunds, W. J.; Cox, M. J.; Ratnam, S.; Muller, C. P. Modeling the impact of subclinical measles transmission in vaccinated populations with waning immunity. *Am. J. Epidemiol.* **1999**, *150*, 1238−1249.
(9) Mossong, J.; O'Callaghan, C. J.; Ratnam, S. Modelling antibody response to measles vaccine and subsequent waning of immunity in a low exposure population. *Vaccine* **2000**, *19*, 523−529.
(10) Putz, M. M.; Bouche, F. B.; de Swart, R. L.; Muller, C. P. 2003. Experimental vaccines against measles in a world of changing epidemiology. *Int. J. Parasitol.* **2003**, *33*, 525−545.
(11) Lamb, R. A. Paramyxovirus fusion: a hypothesis for changes. *Virology* **1993**, *197*, 1−11.
(12) Griffin, D. E. *Measles Virus*, 4th ed., Lippincott: Philadelphia, PA, 2001; Vol. 1.
(13) Dorig, R. E.; Marcil, A.; Chopra, A.; Richardson, C. D. The human CD46 molecule is a receptor for measles virus (Edmonston strain). *Cell* **1993**, *75*, 295−305.

(14) Naniche, D.; Varior-Krishnan, G.; Cervoni, F.; Wild, T. F.; Rossi, B.; Rabourdin-Combe, C.; Gerlier, D. Human membrane cofactor protein (CD46) acts as a cellular receptor for measles virus. *J. Virol*. **1993**, *67*, 6025−6032.
(15) Oldstone, M. B.; Homann, D.; Lewicki, H.; Stevenson, D. One, two, or three step: measles virus receptor dance. *Virology* **2002**, *299*, 162−163.
(16) Tatsuo, H.; Ono, N.; Tanaka, K.; Yanagi, Y. SLAM (CDw150) is a cellular receptor for measles virus. *Nature* **2000**, *406*, 893−897.
(17) Tatsuo, H.; Ono, N.; Yanagi, Y. Morbilliviruses use signaling lymphocyte activation molecules (CD150) as cellular receptors. *J. Virol.* **2001**, *75*, 5842−5850.
(18) Kilby, J. M.; Hopkins, S.; Venetta, T. M.; DiMassimo, B.; Cloud, G. A.; Lee, J. Y.; Alldredge, L.; Hunter, E.; Lambert, D.; Bolognesi, D.; Matthews, T.; Johnson, M. R.; Nowak, M. A.; Shaw, G. M.; Saag, M. S. Potent suppression of HIV-1 replication in humans by T-20, a peptide inhibitor of gp41-mediated virus entry. *Nat. Med.* **1998**, *4*, 1302−1307.
(19) Kilby, J. M.; Lalezari, J. P.; Eron, J. J.; Carlson, M.; Cohen, C.; Arduino, R. C.; Goodgame, J. C.; Gallant, J. E.; Volberding, P.; Murphy, R. L.; Valentine, F.; Saag, M. S.; Nelson, E. L.; Sista, P. R.; Dusek, A. The safety, plasma pharmacokinetics, and antiviral activity of subcutaneous enfuvirtide (T-20), a peptide inhibitor of gp41-mediated virus fusion, in HIV-infected adults. *AIDS Res. Hum. Retroviruses* **2002**, *18*, 685−693.
(20) Lambert, D. M.; Barney, S.; Lambert, A. L.; Guthrie, K.; Medinas, R.; Davis, D. E.; Bucy, T.; Erickson, J.; Merutka, G.; Petteway, S. R., Jr. Peptides from conserved regions of paramyxovirus fusion (F) proteins are potent inhibitors of viral fusion. *Proc. Natl. Acad. Sci. U.S.A.* **1996**, *93*, 2186−2191.
(21) Yao, Q.; Compans, R. W. Peptides corresponding to the heptad repeat sequence of human parainfluenza virus fusion protein are potent inhibitors of virus infection. *Virology* **1996**, *223*, 103−112.
(22) Rapaport, D.; Ovadia, M.; Shai, Y. A synthetic peptide corresponding to a conserved heptad repeat domain is a potent inhibitor of Sendai virus-cell fusion: an emerging similarity with functional domains of other viruses. *EMBO J.* **1995**, *14*, 5524−5531.
(23) Young, J. K.; Hicks, R. P.; Wright, G. E.; Morrison, T. G. Analysis of a peptide inhibitor of paramyxovirus (NDV) fusion using biological assays, NMR, and molecular modeling. *Virology* **1997**, *238*, 291−304.
(24) Cianci, C.; Langley, D. R.; Dischino, D. D.; Sun, Y.; Yu, K. L.; Stanley, A.; Roach, J.; Li, Z.; Dalterio, R.; Colonno, R.; Meanwell, N. A.; Krystal, M. 2004. Targeting a binding pocket within the trimer-of-hairpins: small-molecule inhibition of viral fusion. *Proc. Natl. Acad. Sci. U.S.A.* **2004**, *101*, 15046−15051.
(25) Cianci, C.; Yu, K. L.; Combrink, K.; Sin, N.; Pearce, B.; Wang, A.; Civiello, R.; Voss, S.; Luo, G.; Kadow, K.; Genovesi, E. V.; Venables, B.; Gulgeze, H.; Trehan, A.; James, J.; Lamb, L.; Medina, I.; Roach, J.; Yang, Z.; Zadjura, L.; Colonno, R.; Clark, J.; Meanwell, N.; Krystal, M. Orally active fusion inhibitor of respiratory syncytial virus. *Antimicrob. Agents Chemother*. **2004**, *48*, 413−422.
(26) Weiss, W. J.; Murphy, T.; Lynch, M. E.; Frye, J.; Buklan, A.; Gray, B.; Lenoy, E.; Mitelman, S.; O'Connell, J.; Quartuccio, S.; Huntley, C. Inhalation efficacy of RFI-641 in an African green monkey model of RSV infection. *J. Med. Primatol.* **2003**, *32*, 82−88.
(27) Plemper, R. K.; Erlandson, K. J.; Lakdawala, A. S.; Sun, A.; Prussia, A. J.; Boonsombat, J.; Aki-Sener, E.; Yalcin, I.; Yildiz, I.; Temiz-Arpaci, O.; Tekiner, B.; Liotta, D. C.; Snyder, J. P.; Compans, R. W. *Proc. Natl. Acad. Sci. U.S.A.* **2004**, *101*, 5628−5633.
(28) Plemper, R. K.; Lakdawala, A. S.; Gernert, K. M.; Snyder, J. P.; Compans, R. W. *Biochemistry* **2003**, *42*, 6645−6655.
(29) Plemper, R. K.; Doyle, J.; Sun, A.; Prussia, A.; Cheng, L. T.; Rota, P. A.; Liotta, D. C.; Snyder, J. P.; Compans, R. W. Design of a small-molecule entry inhibitor with activity against primary measles virus strains. *Antimicrob. Agents Chemother*. **2005**, *49*, 3755−3761.
(30) Doyle, J.; Prussia, A.; White, L. K.; Sun, A.; Liotta, D. C.; Snyder, J. P.; Compans, R. W.; Plemper, R. K. Two Domains that Control Pre-fusion Stability and Transport Competence of the Measles Virus Fusion Protein. *J. Virol.* **2006**, *80*, 1524−1536.
(31) Melnikov, A. A.; Palyulin, V. A.; Zefirov, N. S. Generation of molecular graphs for QSAR studies. *Doklady Chemistry* **2005**, *402*, 81−85.
(32) Palyulin, V. A.; Radchenko, E. V.; Zefirov, N. S. Molecular field topology analysis method in QSAR studies of organic compounds. *J. Chem. Inf. Comput. Sci.* **2000**, *40*, 659−667.
(33) Chen, L.; Gorman, J. J.; McKimm-Breschkin, J.; Lawrence, L. J.; Tulloch, P. A.; Smith, B. J.; Colman, P. M.; Lawrence, M. C. The structure of the fusion glycoprotein of Newcastle disease virus suggests a novel paradigm for the molecular mechanism of membrane fusion. *Structure* **2001**, *9*, 255−266.
(34) (a) Eisenberg-Domovich, Y.; Pazy, Y.; Nir, O.; Raboy, B.; Bayer, E. A.; Wilchek, M.; Livnah, O. Structural elements responsible for conversion of streptavidin to a pseudoenzyme. *Proc. Natl. Acad.* Sci. USA **2004**, *101*, 5916−5921 (1RXH); b) Bousset, L.; Belrhali, H.; Melki, R.; Morera, S. Crystal structures of the yeast prion Ure2p functional region in complex with glutathione and related compounds. *Biochemistry* **2001**, *40* 13564−13573 (1K0C); c) Bell, C. E.; Lewis, M. Crystallographic analysis of Lac repressor bound to natural operator O1. *J. Mol. Biol.* **2001**, *312*, 921−926 (1JWL); d) Zhao, Y.; Ke, H. Crystal structure implies that cyclophilin predominantly catalyzes the trans to cis isomerization. *Biochemistry* **1996**, *35*, 7356−7361 (1RMH).
(35) Chambers, C. C.; Cramer, C. J.; Truhlar, D. G. Model for Aqueous Solvation Based on Class IV Atomic Charges and First Solvation Shell Effects. *J. Phys. Chem.* **1996**, *100*, 16385−16398.
(36) Baker, K. A.; Dutch, R. E.; Lamb, R. A.; Jardetzky, T. S. Structural basis for paramyxovirus-mediated membrane fusion. *Mol. Cell* **1999**, *3*, 309−319.
(37) Zhao, X.; Singh, M.; Malashkevich, V. N.; Kim, P. S. Structural characterization of the human respiratory syncytial virus fusion protein core. *Proc. Natl. Acad. Sci. U.S.A.* **2000**, *97*, 14172−14177.
(38) Yin, H. S.; Wen, X.; Paterson, R. G.; Lamb, R. A.; Jardetzky, T. S. Structure of the parainfluenza virus 5 F protein in its metastable, prefusion conformation. *Nature*, **2006**, *439*, doi: 10.1038.
(39) Yin, H. S.; Paterson, R. G.; Wen, X.; Lamb, R. A.; Jardetzky, T. S. Structure of the uncleaved ectodomain of the paramyxovirus (hPIV3) fusion protein. *Proc. Natl. Acad. Sci. U.S.A.* **2005**, *102*, 9288−9293.
(40) Prussia, A.; Plemper, R. K.; Snyder, J. P. unpublished.
(41) Russell, C. J.; Jardetzky, T. S.; Lamb, R. A. Membrane fusion machines of paramyxoviruses: capture of intermediates of fusion. *EMBO J.* **2001**, *20*, 4024−4034.
(42) Halgren, T. Merck molecular force field. 1. Basis, form, scope, parametrization, and performance of MMFF94. *J. Comput. Chem*. **1996**, *17*, 490−519.
(43) Halgren, T. Merck molecular force field. 2. MMFF94 van der Waals and electrostatic parameters for intermolecular interactions. *J. Comput. Chem*. **1996**, *17*, 520−552.
(44) Halgren, T. Merck molecular force field. 3. Molecular geometries and vibrational frequencies for MMFF94. *J. Comput. Chem*. **1996**, *17*, 553−586.
(45) Connolly, M. L. Solvent-accessible surfaces of proteins and nucleic acids. *Science* **1983**, *221*, 709−713.
(46) Connolly, M. L. Analytical molecular surface calculation. *J. Appl. Crystallogr.* **1983**, *16*, 548−558.
(47) Powell, M. J. D. Restart procedures for conjugate gradient method. *Mathematical Programming* **1977**, *12*, 241−254.

JM0602559